FINNISH METEOROLOGICAL INSTITUTE
CONTRIBUTIONS
No. 101

THE SURFACE ALBEDO OF THE ARCTIC FROM SPACEBORNE OPTICAL IMAGERS: RETRIEVAL AND VALIDATION

Aku Riihelä

A doctoral dissertation completed for the degree of Doctor of Science (Technology) to be defended, with the permission of the Aalto University School of Electrical Engineering, at a public examination held at the lecture hall S1 of the school on 17 December 2013 at 12 o'clock (noon).

Finnish Meteorological Institute
Helsinki, 2013

Distribution:
Finnish Meteorological Institute
P.O. Box 503
FIN-00101 Helsinki
Finland
Tel. +358 29 539 1000
Email: aku.riihela@fmi.fi

ISBN 978-951-697-799-0 (paperback)
ISBN 978-951-697-800-3 (pdf)
ISSN 0782-6117

Unigrafia
Helsinki 2013

ILMATIETEEN LAITOS

Julkaisun sarja, numero ja raporttikoodi
Finnish Meteorological Institute Contributions 101
FMI-CONT-101

Julkaisija Ilmatieteen laitos
(Erik Palménin aukio 1)
PL 503
00101 Helsinki

Julkaisuaika 2013

Tekijä
Aku Riihelä

Nimeke
The Surface Albedo of the Arctic From Spaceborne Optical Imagers:
Retrieval and validation

Tiivistelmä

Väitöskirjassa tutkittiin Arktisen lumen ja jään heijastavuuden eli albedon määrittämistä satelliittihavainnoista. Työssä on tuotettu AVHRR-radiometrien mittauksiin perustuvia aikasarjoja sekä operatiiviseen käyttöön että ilmastonmuutostutkimukseen. Aikasarjojen laatu on selvitetty maan pinnan referenssimittauksiin verraten.
Työssä on myös kehitetty menetelmiä parantamaan aikasarjoille laskettujen laatuarvioiden luotettavuutta. Maan pinnan referenssimittausten vertautuvuutta satelliittimittauksiin voidaan työn tulosten perusteella arvioida entistä paremmin.
Väitöskirjan viimeisenä osana on sovellettu työn aiempana osana kehitettyä 28 vuoden aikasarjaa Pohjoisen Jäämeren merijään albedotrendien selvittämiseen. Työssä havaittiin merijäävyöhykkeen keskimääräisen albedon olevan kesäkuukausina laskusuunnassa koko tutkimusjaksolla 1982-2009. Vastaava laskusuunta havaittiin myös jäljelläolevan jääpeitteen albedossa. Tuloksilla on merkitystä Arktisen alueen säteilytaseen, ja yleisemmin alueen ilmaston tutkimukselle.
Väitöskirjan tuloksia voidaan hyödyntää satelliittipohjaisten albedoaikasarjojen ja ilmastomallien varmennus- ja kehitystyössä sekä havaintoihin perustuvassa ilmaston muutosten seurannassa.

Julkaisijayksikkö
Uudet Havaintomenetelmät (UHA)

Luokitus (UDK)
528.8, 551.32, 550.3, 551.52

Asiasanat
Jäätiköt,albedo, lumi, merijää,
kaukokartoitus, lumen ja jään fysiikka

ISSN ja avainnimike
0782-6117 Finnish Meteorological Institute Contributions

ISBN
ISBN 978-951-697-799-0 (nid.)
ISBN 978-951-697-800-3 (pdf)

Kieli
Englanti

Myynti
Ilmatieteen laitos
PL 503
00101 Helsinki

Sivumäärä 167

FINNISH METEOROLOGICAL INSTITUTE

Series title, number and report code
Finnish Meteorological Institute Contributions 101
FMI-CONT-101

Published by Finnish Meteorological Institute
(Erik Palménin aukio 1)
P.O. Box 503
FIN-00101 Helsinki, Finland Date 2013

Author
Aku Riihelä

Title
The Surface Albedo of the Arctic From Spaceborne Optical Imagers:
Retrieval and validation

Abstract

The topic of this dissertation is the study of Arctic snow and ice albedo based on satellite observations. Surface albedo timeseries based on data from the AVHRR instrument family were produced, validated, and analyzed as part of the work. Of note was the production of a 28-year (1982-2009) dataset on global surface albedo from homogenized satellite data, the longest such timeseries to date.

In conjunction with the dataset validation, new methods were developed to improve the reliability of the calculated dataset quality estimate. Specifically, a new method for numerically assessing the representativeness of ground truth observations at the scale of the satellite field of view was introduced.

The final part of this dissertation deals with the application of the 28-year surface albedo dataset in the calculation of sea ice albedo trends over the Arctic Ocean. The results showed a clear negative trend in both the mean composite open water-sea ice albedo and the mean albedo of the remaining sea ice zone. This decrease was linked to decreasing ice concentrations across the ice zone, increased air temperatures and lengthened melt seasons. The results are significant for investigations of the surface energy budget of the Arctic.

The results of this dissertation are of use in the development and validation work of both satellite-based surface albedo datasets and climate models. They created datasets are also useful in observation-based tracking of climate change in the Arctic.

Publishing unit
Earth Observation (UHA)

Classification (UDK)
528.8, 551.32, 550.3, 551.52

Keywords
Glaciers,albedo, snow, sea ice,
remote sensing, snow physics

ISSN and series title
0782-6117 Finnish Meteorological Institute Contributions

ISBN
ISBN 978-951-697-799-0 (nid.)
ISBN 978-951-697-800-3 (pdf)

Language
English

Sold by
Finnish Meteorological Institute
P.O.Box 503
FI-00101 Helsinki, Finland

Pages 167

Preface

Our greatest achievements are never made alone. This dissertation would never have existed if not for the support I had from so many people. I want to thank all the fine folks working in the Earth Observation division at FMI, with a very special thanks to everyone in the Surface Remote Sensing group (a tremendeously helpful and great group of people to dig holes in the snow with). To my mentor and thesis advisor Dr. Terhikki Manninen, a very profound thanks for the years of patience in teaching an engineer how to do geophysical science. I wish to give similarly profound thanks to my second advisor prof. Tuija Pulkkinen, from whom I have learned a wider perspective to science. I wish to also thank my thesis supervisor, prof. Martti Hallikainen, for his insightful comments throughout the work.

The long years of this dissertation have also been supported by some different but no less important groups - firstly the staff of the CM SAF project. My dear colleagues at DWD, KNMI, RMIB, SMHI, MeteoSwiss and UKMO: thank you all, working on this project has been my true higher education in the art and science of remote sensing. Secondly, a shout-out to everyone in the karate club Shoto. There is nothing like a good sparring session to take your mind off work. And to all my friends, thanks for listening my rants about the hardships of being a graduate student. A particular thank you goes to Anniina for all her support.

Most importantly, I have been blessed with a family that has always loved and supported me in whatever I have chosen to pursue. Who could ask for more? Isä, äiti, ja siskoni Ritva, kiitos kaikesta.

Helsinki, August 2013
Aku Riihelä

List of publications

This dissertation is based on the following publications, hereafter referred to as **Papers 1 - 5**.

Paper 1: Riihelä A., Laine V., Manninen T., Palo T., Vihma T., 2010: Validation of the Climate-SAF surface broadband albedo product: Comparisons with in situ observations over Greenland and the ice-covered Arctic Ocean. Remote Sensing of Environment, 114 (11), 2779-2790.

Paper 2: Riihelä, A., Manninen, T., Laine, V., Andersson, K., and Kaspar, F., 2013: CLARA-SAL: a global 28 yr timeseries of Earth's black-sky surface albedo, Atmospheric Chemistry and Physics, 13, 3743-3762.

Paper 3: Riihelä A., and Manninen T., 2008: Measuring the vertical albedo of a subarctic boreal forest canopy. Silva Fennica 42 (5): 807–815.

Paper 4: Manninen, T., Riihelä, A., and de Leeuw, G, 2012.: Atmospheric effect on the ground-based measurements of broadband surface albedo, Atmospheric Measurement Techniques, 5, 2675-2688.

Paper 5: Riihelä, A., Manninen, T., Laine, V., 2013: Observed changes in the albedo of the Arctic sea-ice zone for the period 1982-2009, Nature Climate Change, doi:10.1038/nclimate1963.

In **Paper 1**, I have performed the analysis and validation, and written most of the manuscript. T. Manninen and V. Laine acted as primary scientific advisors and also contributed to the text. T. Palo and T. Vihma provided the Tara reference data and relevant contributions to text.
In **Paper 2**, I have performed the analysis and validation, and written most of the manuscript. T. Manninen and V. Laine acted as primary

scientific advisors and also contributed to the text. K. Andersson created the SAL processing code and F. Kaspar was in charge of the technical processing implementation.
In **Paper 3**, I have done most of the ground measurements and analyzed the results, also writing those parts of the manuscript. T. Manninen planned the work, acted as an advisor for the analysis and contributed to the manuscript text.
In **Paper 4**, I have contributed to the formulation of the study and the manuscript text. T. Manninen was in charge of the analysis and wrote most of the manuscript. G. de Leeuw contributed to the manuscript text.
In **Paper 5**, I have performed the analysis and written the majority of the paper. T. Manninen and V. Laine acted as scientific advisors and contributed to the manuscript text.

Contents

List of Figures

List of Tables

List of Abbreviations

AOD	Aerosol Optical Depth
APP-X	AVHRR Polar Pathfinder Extended
AVHRR	Advanced Very High Resolution Radiometer
BHR	Bihemispherical Reflectance
BRDF	Bidirectional Reflectance Distribution Function
BSRN	Baseline Surface Radiation Network
CLARA-A1-SAL	CM SAF Clouds, Radiation and Albedo - AVHRR First Release - Surface Albedo
CM SAF	Satellite Application Facility on Climate Monitoring
COT	Cloud Optical Thickness
DEM	Digital Elevation Model
DHR	Directional-Hemispherical Reflectance
DOY	Day of Year
ECMWF	European Centre of Medium-range Weather Forecasting
EUMETSAT	European Organisation for the Exploitation of Weather Satellites
FMI	Finnish Meteorological Institute
FMI-ARC	FMI Arctic Research Center
GAC	Global Area Coverage
GrIS	Greenland Ice Sheet
HDRF	Hemispherical-Directional Reflectance Factor
MOD	Melt Onset Date
MOD10A1	Snow albedo product of MODIS
MODIS	The Moderate Resolution Imaging Spectroradiometer
NASA	National Aeronautics and Space Administration
NIR	Near-Infrared
NOAA	National Oceanic and Atmospheric Administration

NSIDC	National Snow and Ice Data Center
OSI-SAF	Ocean and Sea Ice Satellite Application Facility
PPS	Polar Platform System
RMSE	Root Mean Square Error
SAL	Surface Albedo (algorithm name)
SAT	Surface Air Temperature
SHEBA	Surface Heat Balance of the Arctic Ocean
SMAC	Simplified Method for Atmospheric Correction
SNO	Simultaneous Nadir Overpass
SPCTRAL2	Bird Simple Spectral Model
SRTM	Shuttle Radar Topography Mission
SSA	Specific Surface Area
SZA	Sun Zenith Angle
TIROS	Television and Infrared Observation Satellite
TM	Thematic Mapper
TOA	Top Of Atmosphere
USGS	United States Geological Survey
UV	Ultra-violet
VZA	Viewing Zenith Angle

List of Symbols

α	Albedo
$\hat{\gamma}$	Semivariogram estimator
θ_i	Zenith angle of incident (solar) radiation
θ_r	Zenith angle of reflected (solar) radiation
λ	Wavelength
λE	Latent heat flux
Λ	Waveband
ϕ_i	Azimuth angle of incident (solar) radiation
ϕ_r	Azimuth angle of reflected (solar) radiation
ρ	Surface reflectance
τ	Aerosol optical depth
ω_i	Solid angle of incident (solar) radiation
ω_r	Solid angle of reflected (solar) radiation
A	Surface area
C	Sea ice concentration
d	fractional amount of direct radiation flux
D	density
DOY	Day of Year
f_r	Bidirectional Reflectance Distribution Function
G	Ground heat flux
H	Sensible heat flux
I_{dir}	Direct incident radiant flux density (component of S$\downarrow$)
I_{diff}	Diffuse incident radiant flux density (component of S$\downarrow$)
L$\downarrow$	Downwelling longwave radiative flux
L$\uparrow$	Upwelling longwave radiative flux
L_i	Incident radiance

L_r	Reflected radiance
MOD	Melt Onset Date
N	Number of data
r_{eff}	radius of spherical snow grains having equal surface area/volume ratio with actual snow grains
S↓	Incident solar shortwave flux
S↑	Reflected solar shortwave flux
SAT	Surface air temperature

1 | INTRODUCTION

The Sun is essential to life here on Earth. Its radiation provides sustenance for plants and drives the complex climate system of our planet. But not all solar energy that reaches the Earth system is absorbed in it. Both the Earth's surface and the atmosphere above it reflect some of the incident solar energy away. The albedo of the surface is defined as the ratio of reflected to incoming solar radiative flux intensity. Surface albedo varies across materials, from just a few per cent for water or asphalt to approximately 90% for fresh, very small-grained pure snow. This wide range of variation causes significant spatiotemporal variations to the amount of energy that stays within the Earth system and makes surface albedo an important variable for understanding Earth's climate and its changes.

The role of the surface albedo can be mathematically expressed through the energy budget. For a very thin surface in energy balance,

$$(1-\alpha)S\downarrow + L\downarrow = L\uparrow + H + \lambda E + G \tag{1.1}$$

where α is the surface albedo, $S\downarrow$ is the downwelling (incident) solar (shortwave) irradiance on the surface, $L\uparrow$ and $L\downarrow$ are the up- and downwelling longwave radiative fluxes (essentially the thermal radiation of the surface and the atmosphere above), H is the sensible heat flux (heat conducted between the surface and the atmospheric boundary layer), λE is the latent heat flux (heat transferred to or away from the surface by deposition/sublimation), and G is the ground heat flux (heat conducted away within the surface, significant for e.g. water and arid ground).

The role of surface albedo in the Earth's energy budget is particularly important in the polar regions. The albedos of snow and ice vary considerably with the size and shape of the ice grains, contained im-

purities and/or liquid water, atmospheric conditions, and the observation waveband (so-called spectral albedo, Wiscombe & Warren (1980)). Should the snow or ice melt, its albedo will decrease, enhancing solar radiation absorption and causing further melt. The opposite is also true; an increase of snow and ice cover increases albedo and decreases absorbed radiation, causing further cooling. This well-known phenomenon is called the ice albedo feedback (Budyko 1969, Curry et al. 1996). It is, though, but one of several mechanisms influencing the effect that snow and ice albedo have in the surface energy budget of the polar regions. The impact of changes in polar snow and ice albedo is not limited to the polar regions, but can have an effect on the global climate system (Hall 2004).

The need to observe the albedo of the polar regions is therefore obvious, but they are too large, too sparsely populated and environmentally too harsh to enable sufficient spatial or temporal coverage from ground-based or airborne measurements. Optical imagers on board polar-orbiting satellites can observe the vast areas of the Arctic and Antarctic continuously, making them the most cost-effective instruments to retrieve surface albedo with. Exploring the retrieval of surface albedo from space is the first focus of this dissertation. My area of interest shall be the Arctic because of its scientific relevance to global change. The observed retreat and thinning of sea ice cover over the past three decades has gained increasing research attention (Stroeve et al. 2007, Kwok & Rothrock 2009). The relevance of the boreal forest zone for regional and global climate is also being acknowledged (Pielke & Vidale 1995). My main interest will be the determination of snow and ice albedo for the reasons discussed above; however, some attention will be given to the retrievals of surface albedo for the non-snow covered parts of the Arctic. Of the available optical satellite imagers, I will focus on utilization of the Advanced Very High Resolution Radiometer (AVHRR) instrument series. The AVHRR series is used in **Paper 2** of this dissertation to produce a 28-year data record (1982-2009) of global surface albedo called CLARA-A1-SAL (for CM SAF cLouds, RAdiation and Albedo-First Release-Surface ALbedo). The data record has been produced within the Satellite Application Facility on Climate Monitoring (CM SAF), a project of the European Organisation for the Exploitation of Weather Satellites (EUMETSAT).

Correctly accounting for all relevant physical processes in satellite-based remote sensing of albedo to produce an estimate of surface albedo that is close to reality is highly challenging. The process of determining the quality of the estimate is the validation of satellite observations against well-known and reliable reference data. Validation is a crucial step in identifying the strengths and weaknesses in any observational data and its interpretation. Validation of the surface albedo datasets produced in this research is the second focus of this dissertation. I will explore the challenges in validating satellite observations of surface albedo and present the main validation results for the long-term CLARA-A1-SAL albedo dataset.

The third part of this dissertation is dedicated to the study of trends in Arctic sea ice albedo. I will analyze the sea ice albedo from the CLARA-A1-SAL dataset, assess trends in the data and attempt to identify the dominant drivers behind them.

Finally, I will present some concluding remarks and summarize the contributions of this dissertation work to the science of remote sensing of surface albedo.

2 RETRIEVING THE SURFACE ALBEDO OF THE ARCTIC FROM SPACEBORNE OPTICAL IMAGERS

In this chapter, I will describe the process of obtaining an estimate of Arctic surface albedo from spaceborne optical instruments. This starts with the definition and terminology of surface albedo, followed by an overview of the principal reflective properties of snow and ice. Next, I will briefly review the body of literature concerning surface albedo measurements. Then, I will discuss the contribution of this dissertation to the field of satellite-based albedo retrievals, in the form of preparing and validating the SAL algorithm for the creation of operational surface albedo products of the Arctic (**Paper 1**), and a thematic climate data record of surface albedo with an Arctic subset (**Paper 2**).

2.1 Reflectance and albedo: definitions and terminology

It is important to first define the concepts regarding surface reflectivity. Firstly, in optical remote sensing the quantity measured by the instrument(s) is the spectral radiance, defined as the radiant flux in a beam of radiation per unit wavelength, per unit area, per solid angle. It has units of $[Wm^{-2}sr^{-1}nm^{-1}]$.

In a review of reflectance quantities for optical remote sensing, Schaepman-Strub et al. (2006) defines the reflectance of a surface as the ratio between the radiant exitance $[Wm^{-2}]$ and irradiance $[Wm^{-2}]$, which are

both hemispherical quantities. However, especially in remote sensing terminology, surface reflectance is usually defined as a directional quantity describing the relative brightness of a surface. In general terms, reflectance is a function of the illumination and viewing geometry as well as wavelength (Schaepman-Strub et al. 2006):

$$\rho(\theta_i, \phi_i, \omega_i; \theta_r, \phi_r, \omega_r; \lambda) \tag{2.1}$$

where θ and ϕ are the zenith and azimuth angles of illumination (subscript i) or viewing directions (subscript r). ω indicates the solid angle of the cone where the radiation comes from, or is observed from. λ indicates the wavelength(s) of interest.

The definition of the solid angle of incoming/reflected radiation is important. In remote sensing terminology, it is often the case that one speaks of bidirectional reflectance quantities, where in principle both the incoming and reflected radiant fluxes are unidirectional, i.e. defined over a infinitesimally small solid angle. However, Nicodemus (1970) stated that infinitesimal solid angles do not contain measurable amounts of radiant flux. In reality, all optical remote sensing measures the conical reflectance of a surface, i.e. both ω_i and ω_r are finite. A similar argument applies for wavelengths; only a non-infinitesimal waveband (Λ) contains a measurable amount of radiation. As speaking of bidirectional reflectance is nevertheless now standard terminology in optical remote sensing, these terms are used in this dissertation as well. The reader is still advised to keep in mind that the quantities are approximations of true bidirectional reflectances.

If the illumination and observation cones are then expanded to full hemispheres (2 π of solid angle), the formal term for the surface reflectance would be bihemispherical reflectance (BHR), but that is usually supplanted by the term surface albedo. Yet, the definition remains as the ratio between the intensities of the hemispherical radiant flux reflected away from a surface, and the hemispherical radiant flux incident on it. This definition and albedo quantity is the one used in surface energy budget studies and thus in Equation 1.1. Mathematically the simplest definition for surface albedo is:

$$\alpha = \frac{S\uparrow(\Lambda)}{S\downarrow(\Lambda)} = \frac{\int_\Lambda \alpha_s(\lambda) S\downarrow(\lambda) d\lambda}{\int_\Lambda S\downarrow(\lambda) d\lambda} \tag{2.2}$$

where $S\uparrow$ is the reflected hemispherical radiant flux, $S\downarrow$ is the incident hemispherical radiant flux, and Λ is the waveband under consideration (divided into small intervals of $d\lambda$).

For a correct mathematical definition of surface albedo for the remote sensing purposes of this dissertation, it is necessary to define the terminology still further. Ambient illumination (sunlight) consists of both a direct radiant flux component and a diffuse radiant flux component. In theoretical terms, the direct flux is unidirectional, whereas the diffuse flux is perfectly isotropic. Using the reflectance definition of Equation 2.1, we can therefore write the definition of surface albedo under ambient illumination following (Schaepman-Strub et al. 2006):

$$\alpha_{blue-sky} = BHR = \frac{\rho(\theta_{i0},\phi_{i0},2\pi;2\pi;\Lambda)E_{dir}(\theta_{i0},\phi_{i0})}{E_{dir}((\theta_{i0},\phi_{i0}) + \pi L_i^{diff}} + \frac{\pi L_i^{diff}(1/\pi)\int_0^{2\pi}\int_0^{\pi/2}\rho(\theta_{i0},\phi_{i0},2\pi;2\pi;\Lambda)cos\theta_i sin\theta_i d\theta_i d\phi_i}{E_{dir}((\theta_{i0},\phi_{i0}) + \pi L_i^{diff}} \quad (2.3)$$

where θ_{i0},ϕ_{i0} marks the direction of the Sun, E_{dir} is the direct radiant flux intensity, and L_i^{diff} is the diffuse radiant flux density. A shorthand form of the same equation is

$$\alpha_{blue-sky} = BHR = \rho(\theta_{i0},\phi_{i0},2\pi;2\pi;\Lambda)d + \rho(2\pi;2\pi;\Lambda)(1-d) \quad (2.4)$$

where d is the fractional amount of direct radiant flux. In optical remote sensing terms, this definition of surface albedo is often called the blue-sky albedo (Lucht, Hymana, Strahler, Barnsley, Hobson & Muller 2000), marked in the equations with the subscript blue-sky.

For both remote sensing and surface modeling applications it is useful to examine the direct and diffuse radiant flux separately. If the incoming radiant flux is unidirectional, i.e. there are no atmospheric scattering effects, surface albedo is defined as the directional-hemispherical reflectance (*DHR*). Its mathematical expression is

$$\alpha_{BSA} = DHR = \frac{dS\uparrow(\theta_i,\phi_i,2\pi,\Lambda)}{dS\downarrow(\theta_i,\phi_i,\Lambda)} \quad (2.5)$$

$$= \frac{dA\int_0^{2\pi}\int_0^{\pi/2} dL_r(\theta_i,\phi_i;\theta_r,\phi_r;\Lambda)cos\theta_r sin\theta_r d\theta_r d\phi_r}{dS\downarrow(\theta_i,\phi_i,\Lambda)} \quad (2.6)$$

where dA is the surface area, and dL_r is the (directional) reflected radiance. If we further define the Bidirectional Reflectance Distribution Function ($BRDF$) of a surface as (Nicodemus 1970)

$$BRDF = f_r = \frac{dL_r(\theta_i, \phi_i; \theta_r, \phi_r; \Lambda)}{dE_i(\theta_i, \phi_i)} \tag{2.7}$$

and where dE_i is the incident radiant flux from an infinitesimal solid angle (θ_i, ϕ_i), we can write the definition of DHR as

$$= \int_0^{2\pi} \int_0^{\pi/2} f_r(\theta_i, \phi_i; \theta_r, \phi_r; \Lambda) cos\theta_r sin\theta_r d\theta_r d\phi_r \tag{2.8}$$

The interpretation of Equation 2.8 is that, assuming the incident flux is unidirectional, the albedo is determined by simply integrating the (bi)directional surface reflectances (f_r) over the viewing hemisphere. This point of view on surface albedo is highly useful for using remote sensing techniques; we will return to it later. DHR is also called "black-sky albedo" (α_{BSA}) because of the conception of the sky being fully black without atmospheric scattering effects (Lucht, Hymana, Strahler, Barnsley, Hobson & Muller 2000). This term is useful in its descriptiveness and we will use it throughout this summary.

Similarly, if the entire incident radiation flux is diffuse, as might naturally occur under a very thick cloud layer, the expression of BHR can be simplified to (Schaepman-Strub et al. 2006):

$$\alpha_{WSA} = BHR_{ISO} = \rho(2\pi; 2\pi; \Lambda) = \frac{1}{\pi} \int_0^{2\pi} \int_0^{\pi/2} \rho(\theta_i, \phi_i; 2\pi; \Lambda) cos\theta_i sin\theta_i d\theta_i d\phi_i \tag{2.9}$$

The diffuse-flux BHR_{ISO} is also called "white-sky albedo" (α_{WSA}) (Lucht, Hymana, Strahler, Barnsley, Hobson & Muller 2000). Figure 2.1 illustrates the difference between the reflectance quantities DHR and BHR_{ISO}. The reader may note that blue-sky albedo may be calculated based on the black- and white-sky albedos if the fractional amount of direct radiation flux (d) is known, as shown in Equation 2.4.

To illustrate the wavelength-dependent nature of both surface reflectance and incident irradiance, Figure 2.2 shows an example of a typical solar irradiance spectrum at Earth's surface (author's measurement,

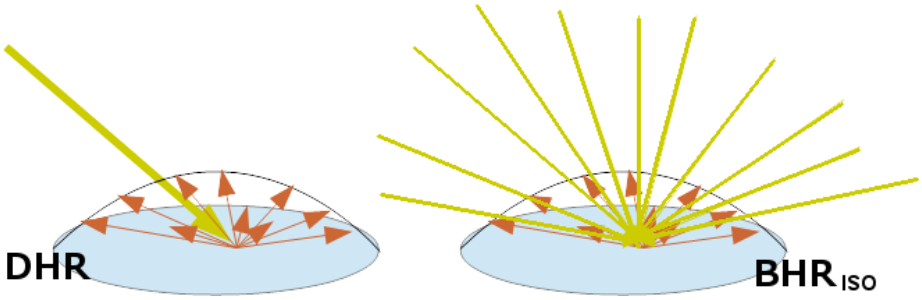

Figure 2.1: Left: a schematic of the directional-hemispherical reflectance (DHR), or black-sky albedo. Right: a schematic of the diffuse-flux bihemispherical reflectance (BHR_{ISO}), or white-sky albedo.

Arctic circle during spring) with typical nadir-viewing reflectance spectra of snow and grass (snow from author's own measurements, grass spectrum courtesy of USGS spectral library (Clark et al. 2007)).

If grass and snow surfaces were isotropic reflectors, the observed surface reflectance would be equal in all directions and the graphs in Figure 2.2 would describe the spectral surface albedo. However, natural surfaces are rarely isotropic reflectors. Snow, in particular, has strongly anisotropic reflectance properties, to which we shall return later. For the purposes of understanding the wavelength dependence of reflectance, it suffices here to consider that if we examine the waveband of visible light (390-700 nm) in Figure 2.2, snow will appear to have a very high reflectance whereas grass will have a low reflectance (with a small reflection peak around 500 nm, explaining its green color). If we consider the full (wavelength-integrated) broadband, both snow and grass have large spectral reflectance (and albedo) over the near-infrared wavelengths, but its effect is dampened by the rapidly decreasing intensity of solar radiation after 800 nm. This is why the broadband albedos of natural surfaces are closer to their visible spectral albedo than the near-infrared albedo, although the latter does provide a contribution.

The absorption peaks in Figure 2.2 also hint at the role that the Earth's atmosphere plays in the determination of surface albedo. Atmospheric constituents such as water vapour or aerosols can either scatter or absorb solar radiation, altering the incident flux at the surface and

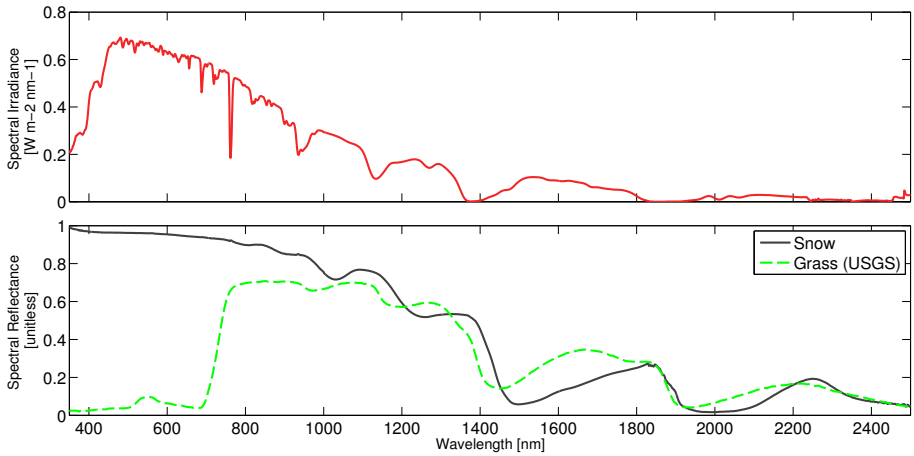

Figure 2.2: Upper panel: example of solar irradiance spectrum at Earth's surface (68 °N, 26 °E, March 2010, SNORTEX campaign (Roujean et al. 2010)). Lower panel: Examples of spectral reflectances of snow (68 °N, 26 °E, March 2010), and grass (USGS spectral library)

thereby also changing the *BHR*. Here, though, it is important to note that the optical properties of natural surfaces are inherent for each material; the black-sky albedo (*DHR*) does not depend on atmospheric conditions as the incident flux is unidirectional and there is no diffuse flux present. In this dissertation, the black-sky albedo is the quantity that is being estimated from satellite observations. Finally, in this dissertation the term reflectance means the directional reflectivity of a surface, following common remote sensing terminology.

2.2 Reflective properties of snow and ice

The ice-air interfaces in a snowpack provide opportunities for the penetrating radiative flux to be reflected or refracted, ultimately leading to a portion of the incident flux escaping the snowpack entirely. The intensity of this escaped flux determines the albedo of the snowpack. As discussed before, the probability of reflection and refraction events depends on the wavelength being studied. It is also intuitively clear that the

more ice-air interfaces exist in a unit volume of snow, the more chances there are for the incident flux to be scattered away. This relationship between the snow grain size and shape and snow albedo is well-known from both theoretical and experimental studies (Warren & Wiscombe 1980, Nolin & Dozier 2000, Kokhanovsky et al. 2005). The relationship is weak in the visible wavelengths, but strong in the near-infrared (Warren & Wiscombe 1980). A useful definition of "snow grain size" for reflective properties studies is a challenging task; without going into the details, we note that defining the optically relevant grain size through the Specific Surface Area (SSA), the ratio between grain size surface area (accessible to gases) and the snow grain mass has yielded useful results (Domine et al. 2006). The relationship between SSA and the physical size of snow grains is given by (Legagneux et al. 2002):

$$SSA = \frac{3}{D \cdot r_{eff}} \tag{2.10}$$

where D is the density of ice and r_{eff} is the radius of spherical snow grains having equal surface area/volume ratio with actual snow grains (Grenfell & Warren 1999). Marking density with D is necessary here to avoid confusion with reflectance, which marked throughout this dissertation with ρ.

Snow is a porous medium and the reflective properties of ice grains change with wavelength, therefore the penetration depth of the incident flux into a snowpack is also wavelength-dependent. Blue wavelengths penetrate deepest, up to 20-30 cm depth - which is why snow inside deep holes in the snowpack appears blue - whereas near-infrared wavelengths only penetrate the snowpack to a depth of a few millimeters before absorption (Li et al. 2001). The considerable penetration depth of visible light also means that the albedo of thin snowpacks (less than 10 cm) is lowered because a part of the penetrating radiative flux survives to meet the darker soil and is more efficiently absorbed, relative to an optically semi-infinite snowpack (Warren & Wiscombe 1980).

The surface-to-mass ratio is largest for fresh, small-grained snow. Sintering, rounding and faceting processes cause the snow grains to grow with time, leading to a lower reflectance and albedo for the snowpack. This ageing process is often called snow metamorphism. Snow metamorphism manifests differently in different snowpacks. It is pri-

marily a function of water vapour available within the snowpack layers, therefore depending on the snow permeability and the temperature gradients between the snow layers (Legagneux et al. 2004, Flanner & Zender 2006). On the other hand, snowfall can reset albedo locally to a high value, commonly cited as 0.84 or 0.85 (Konzelmann & Ohmura 1995, for broadband).

As discussed previously, snow albedo is also a function of the angular distribution of incoming radiation. Commonly this relationship is expressed using the Sun Zenith Angle (SZA); Solar rays entering the snowpack at a large angle of incidence have a higher chance of being scattered in the layers nearest the snow surface, increasing the chances of the photons escaping from the snowpack. The presence of clouds increases the fraction of diffuse incident flux at the surface, which typically, but not always, increases snow albedo (Warren 1982). This effect on snow albedo is sometimes modeled by substituting true SZA with a larger effective SZA under cloudy skies. Clouds also absorb radiation at near-infrared wavelengths more than at UV or visible wavelengths, altering the spectral composition of the (remaining) incoming radiation flux at surface to consist more of visible wavelengths, which snow can reflect more strongly. Multiple reflections between the snowpack and an overhead cloud layer have a similar effect on snow albedo. The net effect of clouds is usually to increase snow albedo underneath.

Another significant driver of snow albedo is the concentration of light-absorbing impurities within the optically accessible layers of the snowpack. Relatively small amounts of impurities can decrease snow albedo significantly in the ultraviolet and visible wavelengths, where light absorption in pure snow is very weak (Warren & Wiscombe 1980). Black carbon, formed by incomplete combustion, is the most effective type of absorbing impurities, but organic carbon and soil dust can account for 20-50% of light absorption caused by impurities in Arctic snow (Doherty et al. 2010).

During the melting season, and generally when the snowpack is warm, meltwater within snow decreases its albedo through filling the spaces between snow grains (and thus decreasing the number of ice-air interfaces) and enhancing grain growth (Dozier 1989). The optical properties of pure ice and water are quite similar in the shortwave waveband, therefore the presence of meltwater within the snowpack affects snow

albedo not directly but indirectly through the mechanisms mentioned (Wiscombe & Warren 1980).

The various drivers of snow albedo act together, but we may consider their effects separately through radiative transfer modeling and the superposition principle. Such a snow albedo parameterization was introduced by Gardner & Sharp (2010), which gives snow broadband albedo as

$$\alpha_{snow-bb} = \alpha_{SSA} + d\alpha_c + d\alpha_{u'} + d\alpha_\tau \tag{2.11}$$

where α_{SSA} is the term describing the snow SSA-albedo relationship, $d\alpha_c$ describes the (negative) effect of light-absorbing impurities, $d\alpha_{u'}$ describes the increase in snow albedo under cloudy skies (as a function of the cloud optical thickness (COT) and effective Sun Zenith Angle), and $d\alpha_\tau$ describes the increase in albedo resulting from the filtering effect of clouds on the incident radiative flux. Cloud optical thickness quantifies light attenuation by cloud droplets in the atmosphere. For the purposes of this thesis, it suffices to illustrate the various components in Figure 2.3, the full parameterization description can be found in Gardner & Sharp (2010).

It should be noted that the Gardner-Sharp parameterization does not take snow surface roughness into account. Several authors argue that surface roughness can have a substantial impact on snow albedo (Carroll & Fitch 1981, Warren 1982), although noting that the surface irregularities have to be several centimeters in size to produce a large effect in the visible albedo. Sastrugi are the most studied roughness features (Warren et al. 1998), but roughness effects between smooth fresh snow and old coarse snow have been experimentally detected (Peltoniemi et al. 2005). However, surface roughness effects are generally difficult to detect in satellite-based albedo measurements due to the coarse spatial resolution, and their effect on surface energy budget is likely not significant (Gardner & Sharp 2010).

As stated in Equation 2.6, surface albedo can be determined by integration of directional reflectances over the viewing hemisphere. The angular reflectance distribution is a function of material properties and wavelength; snow is typically a strong forward scatterer in the visible waveband, but has a more isotropic reflectance distribution in the infrared waveband. Figure 2.4 shows an example of old perennial snow reflectance anisotropy for a selection of wavelengths. Sufficiently dense

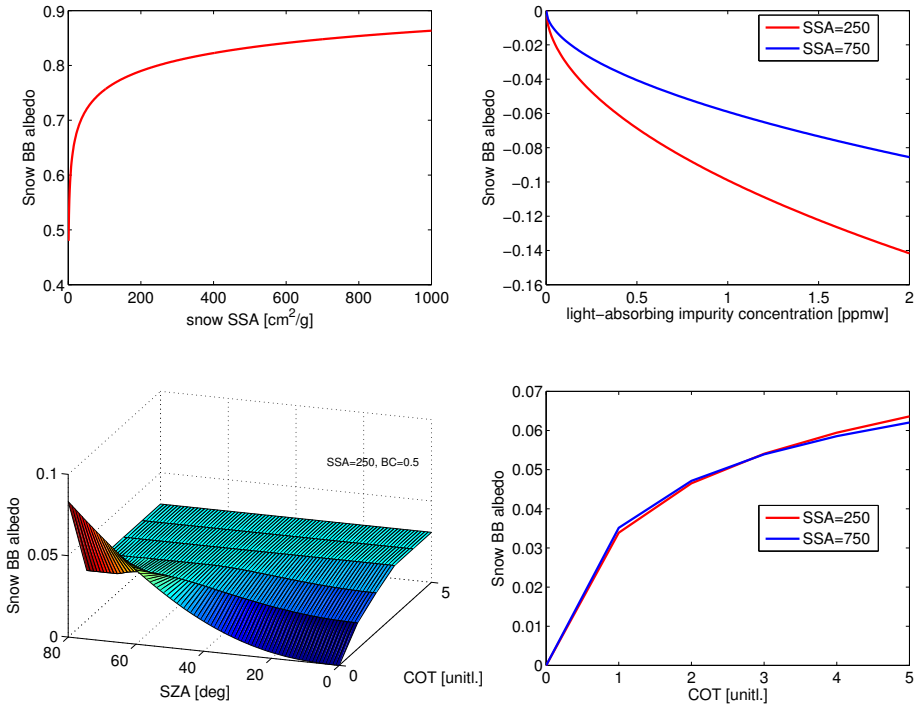

Figure 2.3: Components of snow albedo from the Gardner-Sharp parameterization (Gardner & Sharp 2010). Upper left: Snow broadband albedo as a function of snow Specific Surface Area (SSA) for a Sun Zenith Angle of zero degrees. Upper right: Snow albedo decrease with various levels of light-absorbing carbon contamination. Lower left: Snow albedo increase with increasing cloud optical thickness (COT) and Sun Zenith Angle (SZA). Lower right: snow albedo increase from cloud cover-induced spectral shift in irradiance, impurity concentration used is 0.3 ppmw.

angular reflectance observations can be exploited to obtain a good estimate of snow albedo; this is the basis of the SAL retrieval algorithm **(Papers 1, 2 and 5)** which will be discussed in more detail in section 2.4.

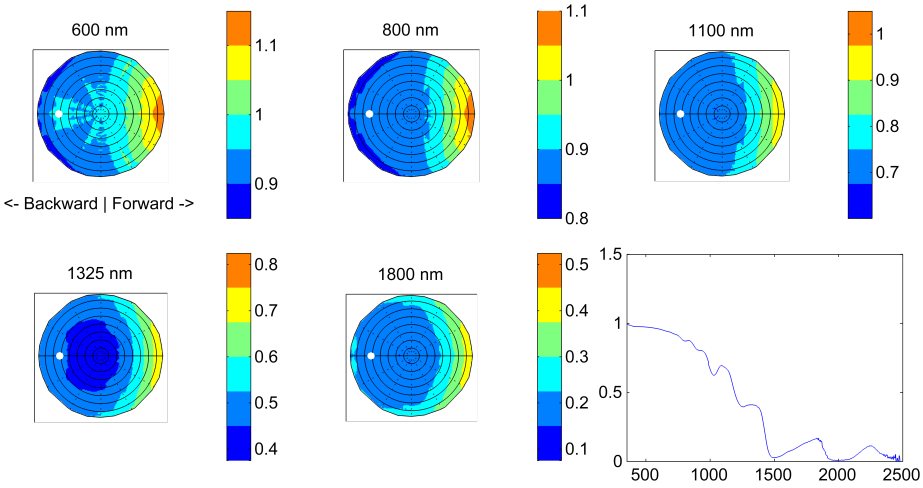

Figure 2.4: An example of the directional reflectance distribution (HDRF) of perennial snow at several wavelengths. Radial distance from plot center indicates increasing viewing zenith angle (0 to 80 degrees). Principal plane is on the x-axis. Sun position marked with a white ball. Lower right panel shows spectral snow reflectance of sample at nadir as a function of wavelength [nm]. Data measured with the FIGIFIGO spectrogoniometer during the RASCALS campaign (Riihelä et al. 2011) on the Greenland Ice Sheet. Measurements and image by Teemu Hakala, FGI. Reproduced with permission.

The albedo of sea ice depends largely on the surface conditions of the ice. If there is a snow cover that is sufficiently thick to be considered optically semi-infinite, then the previous snow albedo discussion applies. The albedo of bare thin ice is firstly sensitive to ice thickness (Maykut 1982), and secondly to ice type - multiyear (bare) ice is brighter than first-year ice thanks to more gas bubbles in the top layers (Perovich 1996). After summer melt onset, melt ponds form on the ice surface, lowering the albedo. The size and depth of the melt ponds is the con-

trolling factor in the albedo decrease. Drainage of the melt ponds can temporarily reset the albedo to a higher level (Perovich & Polashenski 2012). In the autumn, refreezing begins to increase the surface albedo again, closing the seasonal cycle (Perovich & Polashenski 2012). In very cold conditions (ice temperature less than -23 °C), salt crystals begin to condense in the brine inclusions within the top snow/ice layers (hydrohalite precipitation), which increases the ice albedo (Light et al. 2004). However, as the summer melt of the snow and ice dilutes salt crystals in brine and later flushes them away, their overall effect on sea ice albedo is very small.

2.3 A literature review of snow and ice albedo measurements

In this section, we will review a selection of past scientific literature on measurements of snow and ice albedo. This review is by no means exhaustive; its purpose is to provide the reader with a general overview on the development of the field, and to provide a starting point of references for the reader interested in pursuing the topic further. As the dissertation focus is on the Arctic, I will omit literature relating to surface albedo measurements from geostationary satellites to maintain brevity and clarity.

Published in situ measurements of the reflective properties of snow have a history of nearly a century. Following the development of the modern pyranometer (Ångström 1919), snow albedo measurements were published probably for the first time by Ångström (1925). This was soon followed by Kalitin (1930), describing measurements taken near Leningrad in the Soviet Union in 1929. Both studies obtained results agreeing very well with current estimates for snow albedo, recognized the variability of albedo with the condition of the snow cover, and noted that fresh snow is brightest of all observed natural surfaces. As for perennial snow, the albedo in Antarctica was first measured systematically by Liljequist (1956) at Maudheim near the coast of Queen Maud Land. Similar measurements were undertaken on the Greenland Ice Sheet by Ambach (1985) in 1959 and 1967. Published in situ measurements of the reflective properties of snow have a history of nearly a century. Fol-

lowing the development of the modern pyranometer (Ångström 1919), snow albedo measurements were published probably for the first time by Ångström (1925). This was soon followed by Kalitin (1930), describing measurements taken near Leningrad in the Soviet Union in 1929. Both studies obtained results agreeing very well with current estimates for snow albedo, recognized the variability of albedo with the condition of the snow cover, and noted that fresh snow is brightest of all observed natural surfaces. As for perennial snow, the albedo in Antarctica was first measured systematically by Liljequist (1956) at Maudheim near the coast of Queen Maud Land. Similar measurements were undertaken on the Greenland Ice Sheet by Ambach (1985) in 1959 and 1967.

It was recognized early on that ground measurements could not cover sufficient area to provide climatologically valuable estimates of surface albedo. Thus thoughts turned to airborne measurements. An extensive flight campaign of albedo measurements over the continental U.S. was described by Kung et al. (1964). They found, correctly, that snow albedo increases with increasing snow depth up to 10-15 cm depths, after which the albedo levels off. They also noted that the albedo of snow-covered forest stands appears to relate to the canopy density, tree species mixture, and differences in the condition of the snow cover.

Airborne flight campaigns of albedo measurements might have become common if not for the advent of satellite remote sensing. Nordberg et al. (1962) and Fritz et al. (1962) published results of reflectivity measurements of the Earth's surface-atmosphere system (now known as Top-of-Atmosphere [TOA] reflectance) based on the TIROS (Television and InfraRed Observation Satellite) III experimental meteorological satellite. These first studies, although pioneering, had very limited spectral, spatial or temporal coverage. A few years later, Vonder Haar & Suomi (1969) and Raschke et al. (1973) were already able to provide global maps of the broadband albedo of the Earth system, including the polar regions. Raschke et al. even estimated global surface albedo by finding the minimum TOA albedo per grid cell in their observations. While this approach was relatively simplistic compared to modern atmospheric correction algorithms, it represented the first step in obtaining surface albedo from satellite observations.

Polar-orbiting sun-synchronous satellites were found to be the most appropriate for cryospheric monitoring, and continuous observation ca-

pabilities were introduced in the NOAA satellite series with the AVHRR instrument family. Robock & Kaiser (1985) summarized early measurements of bidirectional snow reflectance from AVHRR. Dedicated algorithms for deriving snow and ice albedo began emerging soon; DeAbreu et al. (1994) and Lindsay & Rothrock (1994) published Arctic sea ice albedo retrieval algorithms, as did Stroeve et al. (1997) for snow on the Greenland Ice Sheet. Key et al. (2001) presented an algorithm for snow and ice albedo determination for both clear- and cloudy sky conditions from AVHRR Polar Pathfinder data (Maslanik et al. 1997). This algorithm was later implemented in the creation of the AVHRR Polar Pathfinder Extended (APP-X) dataset, which has been the most commonly used long-term source for satellite-based surface albedo data over the polar regions.

The albedo retrieval capabilities of the polar-orbiting satellite family were further advanced by the launch of the MODIS instruments on board the Terra and Aqua satellites in 1999 and 2002 (Salomonson et al. 1989). The MODIS instrument features better spatial resolution and a larger selection of imaging channels than the AVHRR, as well as a continuous on-board calibration of the measurements. The retrieval scheme for snow albedo from MODIS was developed by Klein & Stroeve (2002) and implemented as the MOD10A1 snow albedo product.

In the last decade, the available satellite products and datasets have grown long enough to enable studies related to cryospheric climate trends from satellite retrievals. To provide some examples, I mention studies of decadal Arctic albedo changes such as Laine (2004) for sea ice, (Wang & Key 2005) for the whole Arctic, Comiso (2001) combining microwave and optical satellite data, and Box et al. (2012) for the Greenland Ice Sheet. This dissertation continues in the direction pointed by these studies.

Table 2.1: Main characteristics of the AVHRR/3 sensor

Channels	1: 0.58 - 0.68 μm 2: .725 - 1 μm 3A: 1.58 - 1.64 μm 3B: 3.55 - 3.93 μm 4: 10.3 - 11.3 μm 5: 11.5 - 12.5 μm
Swath width	2600 km
Spatial sub-nadir resolution	1.09 km (LAC) 4.36 km (GAC)

2.4 Retrieving the surface albedo of the Arctic with AVHRR and the SAL algorithm

From this point onwards, we begin to consider the contributions that this dissertation brings to the field of remote sensing. **Paper 1** details the SAL albedo retrieval algorithm, which is used again for deriving a long-term albedo dataset in **Paper 2**. It should be noted that while the development of the SAL algorithm itself is not a part of this dissertation work, its validation and deployment to Arctic climate monitoring are - therefore we will briefly summarize the AVHRR instrument capabilities and SAL algorithm first.

The Advanced Very High Resolution Radiometer observes the Earth's surface at six separate channels (the AVHRR/3 version) between 0.58 and 12.50 μm. All imaging channels have a sub-nadir spatial footprint of 1.09 km at surface. The instrument is of the "whisk-broom" type, meaning that a rotating mirror moves the light detector focus continuously over the surface beneath the satellite. While this continuous scanning limits instrument sensitivity for any single imaged scene (pixel), it offers a wide imaged swath per orbit in exchange. From a flight altitude of approximately 830-870 km, the AVHRR achieves an imaging swath width of approximately 2600 km.

Due to limitations in onboard data storage, the full-resolution data is typically only available on a regional level via local receiving stations.

Global coverage for the full AVHRR family coverage period is available through the reduced-resolution Global Area Coverage (GAC) data. The GAC data consists of an average of 4 out of every 5 pixels in an AHVRR full-resolution swath, and 1 out of 3 imaged swaths. Thus, its sub-nadir resolution is roughly 4.4 km. The operational SAL products (as described in **Paper 1**) are based on full-resolution AVHRR data; the CLARA-A1-SAL dataset (as described in **Paper 2**) is based on AVHRR-GAC data.

In general, the retrieval of surface albedo from satellites requires solving the following problems:

1. Many image pixels are partly or completely contaminated by cloud cover. The reflectance properties of most clouds also resemble snow quite closely. Both of these issues must be solved to exempt the cloud-contaminated pixels from the retrieval and to identify cloud-free snow and sea ice pixels for later computation (*cloud mask problem*)

2. Topography effects on radiometry and geolocation of satellite data need to resolved for accurate albedo determination over rough, mountaineous terrain (*topography problem*)

3. The radiances contain a contribution from the absorption and scattering mechanisms of the atmosphere between the instrument and the observed surface (*atmospheric problem*)

4. The radiance observed by the satellite instrument represents only a single viewing and illumination geometry (*BRDF problem*)

5. The observed radiances are limited in wavelength by the instrument's spectral response (*narrow-to-broadband conversion problem*)

Some retrieval schemes also choose to normalize the satellite measurements to correspond to a predescribed Sun Zenith Angle. In the operational SAL processing we chose to use such a procedure (Briegleb et al. 1986), whereas the CLARA-A1-SAL data were not normalized, but rather represent the mean distribution of SZAs for each grid cell and time period.

These problems are solved in the SAL algorithm following the processing flow depicted in Figure 2.5. The identification of cloudy pixels in the AVHRR images is performed by the PPS software package in the pre-processing stage. Details on the AVHRR-PPS package and cloud mask derivation can be found in Dybbroe et al. (2005). Identification of snow, ice and clouds is accomplished through a series of dynamic thresholding tests of the observed radiances, achieving a success rate of approximately 90% for Arctic summer clouds (Karlsson & Dybbroe 2010). At this point, the radiances are also converted to Top-of-Atmosphere (TOA) reflectances by normalizing them with the exoatmospheric irrandiance (adjusted by the Sun-Earth distance variation). AVHRR channels 1 (0.58-0.68 μm) and 2 (0.725-1 μm) are used as SAL input.

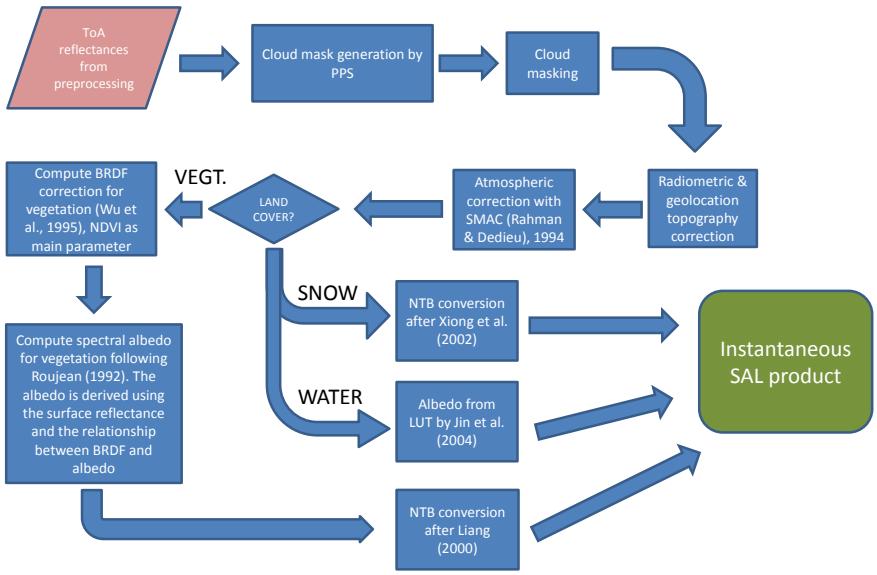

Figure 2.5: The Surface ALbedo (SAL) algorithm flow, as used in the processing of the CLARA-A1-SAL dataset.

Topography effects in satellite-based surface albedo retrievals are a

significant source of uncertainty in mountainous terrain (e.g. the Alps or Himalaya). In SAL, topography effects on radiometry are calculated by using a high-resolution digital elevation model (DEM) from the Shuttle Radar Topography Mission (SRTM) to identify the number and disposition of slopes within an AVHRR image pixel, and calculating reflectance anisotropy effects for each slope separately. Topography effects on geolocation are corrected for by calculating true pixel coordinates given realistic topography, and comparing to the given coordinates calculated by the preprocessor software assuming a flat ground surface. If the discrepancy is more than half a pixel versus true terrain, the coordinates are corrected. The full equations are not reproduced here, more details on the topography correction can be found in Manninen et al. (2011) and on SRTM DEM in Farr et al. (2007).

The atmospheric correction of satellite-observed reflectances is an important and necessary step to bring the observations to surface reflectance level. First- and multiple-order molecular and aerosol scattering, as well as absorption effects need to be compensated for to retrieve a good estimate for the surface reflectance. Atmospheric correction also depends on the viewing and illumination geometry of the satellite image - at large angles, the path length of the solar radiation through the atmosphere is large, making the correction more difficult. The Simplified Method for Atmospheric Correction (SMAC) algorithm is used for atmospheric correction in all SAL product calculations (Rahman & Dedieu 1994). The algorithm accounts for gaseous absorption, as well as Rayleigh and aerosol scattering. To avoid the most problematic correction cases with large viewing or illumination angles, the SAL algorithm uses cut-offs of 60 degrees for the Viewing Zenith Angle (VZA), and 70 degrees for SZA.

A robust atmospheric correction requires knowledge of the atmospheric constituents. Generally speaking, the amounts of water vapour and aerosols affect satellite radiances most, with ozone concentrations and the columnar air mass playing minor parts. It is possible to attempt a simultaneous single image-based retrieval of surface albedo and the parameters needed for the atmospheric correction (Loew & Govaerts 2010, Kaufman & Gao 1992), but such an approach is not optimal for AVHRR because of the large bandwidth and low number of the imaging channels. In SAL processing, water vapour input is based on atmospheric model

runs made at the European Centre of Medium-range Weather Forecasting (ECMWF). The question of aerosols, however, is more complicated.

The commonly used quantity to describe aerosol concentration is the Aerosol Optical Depth (AOD, sometimes also called Aerosol Optical Thickness), which is the integrated extinction coefficient (of radiation) over a vertical air column of unit cross section. Aerosol concentrations in the atmosphere vary considerably, being generated both by natural sources (e.g. dust storms over deserts) and anthropogenic sources (e.g. combustion byproducts). A wrong choice of AOD can substantially bias the satellite-based surface albedo retrieval. The issue is also complex because land cover affects aerosol scattering and absorption intensity through multiple scattering between the surface and the atmosphere - aerosol effects are potentially more severe over bright snow and ice surfaces (Li & Garand 1994, Kaufman & Tanré 1996).

In SAL processing, a conscious choice was made to avoid aerosol models, instead utilizing a constant background AOD value (0.1 at 550 nm) until a robust, observation-based global aerosol dataset of sufficient duration is available. The validity of this choice was evaluated with RTM calculations as a part of **Paper 2**. The main findings were that a) using a background AOD value of 0.1 is an acceptable choice over the polar regions, where prevailing AODs are generally close to that value and vary only slightly over time (Tomasi et al. 2012), and b) the broadband surface albedo estimates from SAL are not critically sensitive to typical AOD variations over most landmasses in the Northern Hemisphere. The main reason for this is that the narrow-to-broadband albedo conversion in SAL gives substantially greater weight to the retrieved NIR waveband albedo, limiting aerosol effects on the result since aerosols are less effective scatterers at NIR wavelengths than visible wavelengths (Kaufman & Tanré 1996). The analysis in **Paper 2** also confirmed the RTM calculation results with direct comparisons to MODIS black-sky albedo products for which a dynamic aerosol correction is implemented. The difference showed low sensitivity to AOD (taken from an independent dataset) until larger values of over 0.35 were reached.

After the atmospheric correction, the next computation stage depends on the type of surface in question. For land surfaces, spectral albedo is calculated in conjunction with the BRDF correction following the approaches of Roujean et al. (1992) and Wu et al. (1995). The re-

quired broadband albedo is then derived through a narrow-to-broadband conversion algorithm (Liang 2000).

The retrieval of broadband albedo for snow and ice is based on a different approach. The spectral (directional) surface reflectances are directly converted into broadband reflectances (using the algorithm by Xiong et al. (2002)), reprojected into the desired end product grid, and averaged over a suitable timeframe for each grid cell. In essence, we exploit the varying AVHRR imaging geometry, high data availability over polar regions, and averaging to a coarser end product grid to sample the reflectance hemisphere densely enough to retrieve an albedo estimate. On a conceptual level, one may consider that the method modifies Equation 2.6 replacing the hemispherical integral of bidirectional surface reflectances with an averaging of dense reflectance samples. This approach is novel and its validation was the main task in **Paper 1** for the operational SAL product, and also in **Paper 2** for the 28-year CLARA-A1-SAL timeseries.

A similar type of approach is used in the determination of MODIS land surface albedo (Lucht, Schaaf & Strahler 2000), where multiangular satellite observations are fitted into a kernel-based reflectance-to-albedo model. As the reflectance signatures of snow and ice vary widely depending on surface conditions (Warren 1982), which are difficult to determine from the satellite image alone, it was decided not to attempt this approach for snow and ice albedo calculations in SAL.

The multiangular reflectance averaging approach places the following limitations on the data: Firstly, the reflectance hemisphere must be sampled with sufficient density for the averaging to produce a good estimate of albedo. The viewing sampling density of the AVHRR observations of Arctic snow and ice was evaluated in **Papers 1 and 2**. The sampling density was found to be sufficient when averaging the observations over a period of a week or a pentad (5 days), and quite good when averaged over a period of one month. As albedo studies relate primarily to climatology, the monthly mean albedo is often the most desired quantity - meaning more available data per SAL product, and resulting in a more robust albedo retrieval. Figure 2.6 illustrates the achievable angular sampling for monthly means in the CLARA-A1-SAL dataset.

Secondly, rapid changes in surface conditions could potentially bias the resulting albedo estimate if e.g. high cloudiness were to limit the

amount of available data for the timeperiod. However, the narrow-to-broadband conversion algorithm (Xiong et al. 2002) self-adjusts for varying snow and ice conditions, mitigating this issue.

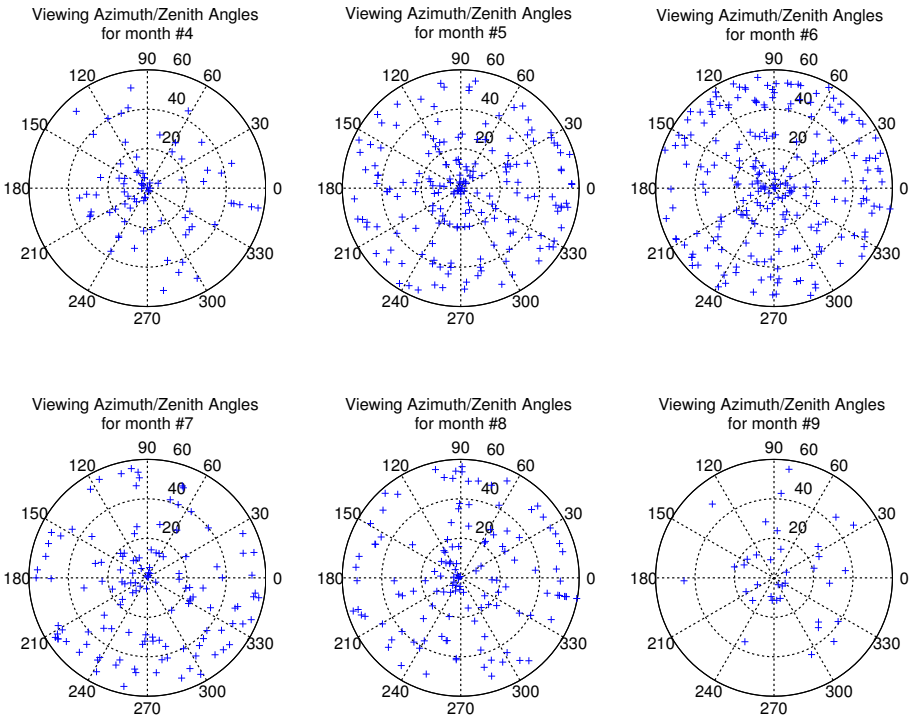

Figure 2.6: An example of the viewing zenith and azimuth angle sampling in the 28-year CLARA-A1-SAL dataset. The radial direction in the subplots shows viewing zenith angle, azimuthal direction equates to azimuth viewing angle. The site in question is the Summit Geophysical Observatory on the Greenland Ice Sheet, the period is the year 2005.

Figure 2.7 shows examples of the Arctic surface albedo from CLARA-A1-SAL. The Arctic products are released at a spatial resolution of 25 kilometers in a Lambertian equal-area grid. The figure shows the July monthly mean albedos from 1982 and 2009, the first and last years of the dataset. The figure highlights some of the changes in the sea ice zone albedo, to which we will return in detail in Chapter 4.

The amount of available AVHRR data was considerably lower in the 1980s when only one or two satellites were operational simultaneously. This indicates that the early period mean albedos can exhibit some artifacts where misclassifications of clouds as snow and ice co-occur with cloudy periods that limit the number of available observations, increasing the weight of sporadic poor-quality retrievals. This issue was resolved in the operational SAL algorithm with the inclusion of OSI-SAF sea ice concentration mask (**Paper 1**). A long-term sea ice mask will be included in the next release of the CLARA-SAL dataset to improve quality for the early period.

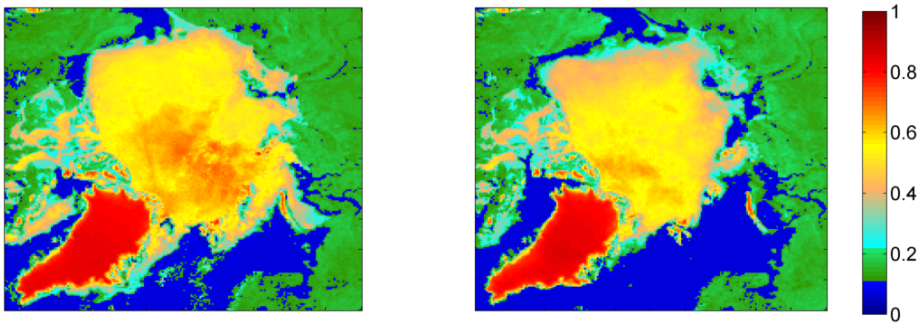

Figure 2.7: Left: July 1982 monthly mean black-sky surface albedo over the Arctic. Right: July 2009 monthly mean black-sky surface albedo over the Arctic. Data from CLARA-A1-SAL dataset (**Paper 2**).

For consideration of the Arctic sea ice albedo trends that I will present in Chapter 4 (based on **Paper 5**), it is important to note that the amount of available overpasses for the mean albedo retrieval was still sufficiently large even in the early period. Figure 2.8 displays the increase in AVHRR data through the 28 years of CLARA-A1-SAL coverage. Even in the 1980s, there were on average 500 successful satellite observations per grid cell for the mid-summer months, and approximately 200 for August.

Before finishing this discussion on the retrieval technique for Arctic surface albedo, one last mention needs to be made. In climate applications, the correct identification of trends in data is of crucial importance. The AVHRR family is one of the few series of instruments that have

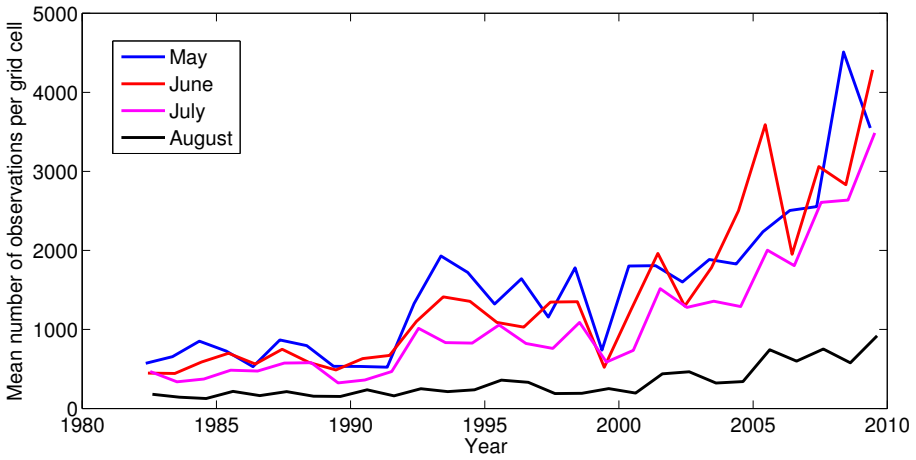

Figure 2.8: Average number of observations per grid cell over the Arctic sea ice zone (area with over 15% ice concentration) in CLARA-A1-SAL.

provided data on timescales which begin to be useful for climate model verification and development. However, a lasting source of lament has been the fact that the individual AVHRR instrument calibrations were not consistent and tended to drift post-launch with sensor aging (Stowe et al. 2002). The work by Heidinger et al. (2010) led to an intercalibration procedure for the entire AVHRR instrument family from NOAA-7 to METOP-A, utilizing MODIS as a stable reference through Simultaneous Nadir Overpasses (SNO) when available, and known stable-albedo ground targets as an alternative reference. This procedure was applied to the CLARA-A1-SAL dataset and is a vitally necessary precursor to this dissertation's study of Arctic sea ice albedo trends in **Paper 5** and therefore deserves a special mention here.

3 VALIDATION OF THE SATELLITE-BASED SURFACE ALBEDO RETRIEVALS

In this chapter, I will present some notable challenges in verifying the quality of the satellite-based surface albedo retrievals described in the previous chapter, and summarize the contributions of the dissertation to this topic. I will first consider two particular problems in the albedo retrievals and then review the validation results obtained using the SAL algorithm with a long-term AVHRR radiance dataset, as described in Section 2.4.

3.1 The representativeness problem

Surface albedo retrievals from typically used satellite data have ground footprints ranging from 900 m^2 (Landsat TM) to 18.15 km^2 (AVHRR GAC at nadir), even without considering spatial averaging of end products. But the ground reference data on surface albedo usually comes from pyranometer pairs installed at close to ground level, having an approximate footprint of several hundred to a thousand square meters, depending on installation height and sensor angular response. This large disparity in resolution poses a question whether even a perfect retrieval algorithm would produce a satellite-derived albedo that would agree perfectly with the ground reference because of the difference in measurement areas.

The problem of spatial representativeness of ground observations of albedo has drawn considerable research attention (e.g. Lucht, Hymana, Strahler, Barnsley, Hobson & Muller 2000, Liang et al. 2002, Susaki

et al. 2007, Román et al. 2009). Many recent attempts at enabling the validation of satellite-derived albedo products from ground truth data have revolved around a combined usage of higher-resolution satellite data and empirical semivariograms. In geostatistics, semivariograms are used to describe the spatial autocorrelation of measurements. Semivariograms illustrate the similarity of measurements at increasing distance (lag) relative to a reference point and therefore quantify the representativeness of a single site for a larger area. The empirical semivariogram (also called semivariogram estimator) is calculated as (Matheron 1963)

$$\hat{\gamma}(h) = \frac{1}{2N(h)} \sum_{i=1}^{N(h)} [z(x_i + h) - z(x_i)]^2 \tag{3.1}$$

where N(h) is the number of data pairs (z(x_i + h), z(x_i)) at distance h from each other.

In **Paper 2**, I developed a method to rank the representativeness of validation sites using semivariogram estimators and Landsat TM imagery. The principle of the method is that the differences in surface reflectance relative to the validation site across a Landsat image can be integrated to obtain a quantitative measure of site representativeness. Specifically, I calculate the average NIR waveband (TM channel 4) surface reflectance of all TM pixels at each (increasing) lag distance from the site coordinates, and subtract the site surface reflectance to derive the average reflectance difference. This procedure is repeated until reflectance differences have been calculated up to a lag distance equal to half of the coarser (in this case AVHRR GAC) satellite resolution. I then integrate the resulting set of semivariogram estimators to obtain the representativeness indicator. That is then used as a weight in the determination of (average) albedo retrieval capability. If the validation site is representative of its surroundings, the semivariogram estimator integral will have a low value, and vice versa.

Figure 3.1 illustrates the calculation: upper subplot shows the calculated semivariogram estimators at each lag distance (multiples of 30 meters). Lower subplot visualizes a selection of landsat pixels at various lag distances for visual verification.

The method is very similar to the ones developed by Susaki et al. (2007) and Román et al. (2009), but is simplified. Most previous approaches keep to the semivariogram theory, interpreting the result through

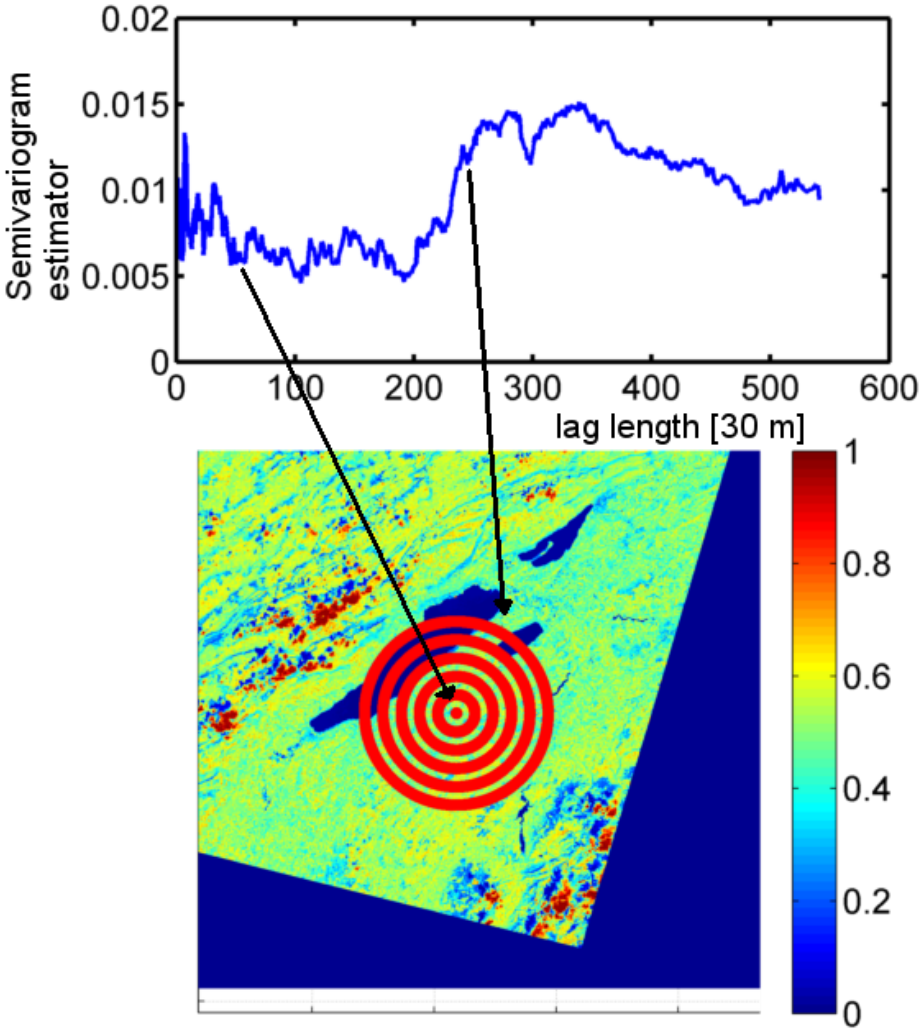

Figure 3.1: Example of calculated semivariograms in **Paper 2**. Site is Payerne in Switzerland. Increase in mean surface reflectance difference (upper subplot) is clearly seen when the variogram is calculated at lag distance of 250 [Landsat pixels] as a result of the influence of nearby Lac du Neuchâtel in the middle of lower subplot (Landsat TM channel 4 image).

a variogram model fit and using the model parameters, commonly range and sill, as the resulting indicators.

Strictly speaking, my use of NIR surface reflectances limits the scope of the method as-is to vegetated terrain sites in absence of snow. If the NIR surface reflectances were replaced with albedo estimates, then the method could be applicable also for (partly) snow-covered sites. NIR waveband surface reflectances are a justifiable substitute for broadband albedo in the case of vegetated surfaces and AVHRR-based retrievals using the narrow-to-broadband conversion algorithm by Liang (2000), which gives greatest weight to NIR waveband over vegetated terrain. Also, aerosol scattering effects are weaker in the NIR waveband compared to visible wavelengths, meaning that the Landsat surface reflectance data from the NIR channel is likely more reliable.

When the site or its surroundings are snow-covered, the situation is different. In the case of complete snow-cover and in absence of forest stands, the homogeneity of snow reflectance over the scale of a few kilometers is typically so large that site representativeness can be considered assured. Thus, the validation effort in **Paper 2** did not include representativeness calculations for sites over perennial snow on the Greenland Ice Sheet or Antarctica.

Partial snow cover and/or snow cover on trees complicates the site representativeness assessment further. While this method could be extended to partial snow cover given full broadband albedo calculation from the high-resolution image, the availability of e.g. Landsat data over a given area at a given time tends to be uncertain due to revisit time limitations and cloudiness. Also, the spatial coverage of partial snow cover is variable in the melting season, limiting the true representativeness of a single variogram estimator calculation for a site.

The case of in situ albedo measurement representativeness for forest stands with or without snow cover is a problem which warranted a separate study (**Paper 3**). I will summarize the results of that study next.

3.2 Forest albedo at stand versus ground level

The interaction of solar radiation with forest canopies is a complex process. The albedo of a forest stand is determined by multiple-order scattering processes between the forest understory and the canopy (Kuusk 2001, Manninen & Stenberg 2009). The presence of snow cover on the ground and on the trees further increases the complexity of the radiative transfer process, increasing forest stand albedo and increasing its variability (Betts & Ball 1997, Kuusinen et al. 2012).

The large boreal forest zone with its seasonal snow cover is an important part of the Arctic and even global climate systems, having a sufficiently large area to significantly influence global albedo. However, the validation of satellite-based albedo retrievals is made difficult by the sparsity of above-canopy albedo monitoring sites. This motivated the study in **Paper 3** to assess the possibilities to estimate the surface albedo of a forest stand from ground level measurements.

To that end, a measurement apparatus was constructed by FMI technical staff and myself at the FMI Arctic Research Center (FMI-ARC) in Sodankylä which enabled an albedo-meter to be raised and lowered within a Scots pine forest stand of roughly 12 m high. The present understory was a mix of sand, heather and other typical understory species of the area. Measurements were taken during summer 2006 and winter 2007. The summer measurements were characterized by persistent cloud cover over the site; the winter measurements were performed when there was heavy snow cover on the trees. The measurements generally took place so that they were centered on midday, the exception being the second profile measured on 2.8.2006 in the afternoon.

The measured forest stand albedo over the canopy (approximately 0.1 in summer and 0.2 in winter) was in line with previous studies (Betts & Ball 1997). The vertical albedo profiles were form-wise similar and appeared to match a power-law distribution best, although the best-fit regression parameters varied significantly. Figure 3.3 summarizes the measurement results. Why is the best agreement found in power-law behaviour? Because the data characterizes only one site and the focus of the study was on demonstrating if ground observations could be repeatably related to top-of-canopy albedo, no firm conclusions on the causes

Figure 3.2: A photograph of the measurement arrangement in **Paper 3**.

of the apparent power-law behaviour may be drawn from the data. If we allow for some speculation, it may be noted that phenomena following power-law behaviour are common in forest structure studies. For example, Dobson et al. (1995) showed that the dry biomass of a boreal North American forest was related to Synthetic Aperture Radar (SAR) backscattered power (at two wavebands) by a power-law relationship. On a more general note, West et al. (1999) stated that scaling relationships in biological delivery networks, such as forest canopies, will obey power-law relationships owing to their fractal nature. Also, the albedo measurements taken in **Paper 3** were broadband, therefore they need not necessarily conform absolutely to the exponential forms of spectral radiation attenuation.

The winter measurements were few in number, and their results showed more scatter. This was most likely a result of the low Sun elevation, leading to long path lengths of incident radiation within the canopy, combined with snow cover on the trees, which enhance multiple reflection processes within the canopy. It is noteworthy that despite the fact that surface albedo at the understory level is comparable to the albedo of a snow field, the albedo of the forest stand over the canopy still reduces to approximately 0.2. This behaviour has been noted in other studies (Betts & Ball 1997), although also higher forest stand albedos have been observed for Finnish boreal forests in winter (Kuusinen et al. 2012).

The study thus showed that, in principle, forest stand albedo is related to the understory-level albedo, alhtough a single albedo measurement at the forest floor is insufficient to predict the forest stand albedo. Forest structure, the presence of snow and illumination conditions all play a part in the relationship. Thus, more modeling and observation studies are necessary to provide a robust solution to the problem of obtaining applicable validation data for forest albedo from understory albedo measurements.

3.3 Blue-sky vs. black-sky albedo: The impact of atmospheric effects

The satellite-derived albedo estimated in this dissertation is the black-sky albedo, equivalent to a situation where the incoming radiant flux is

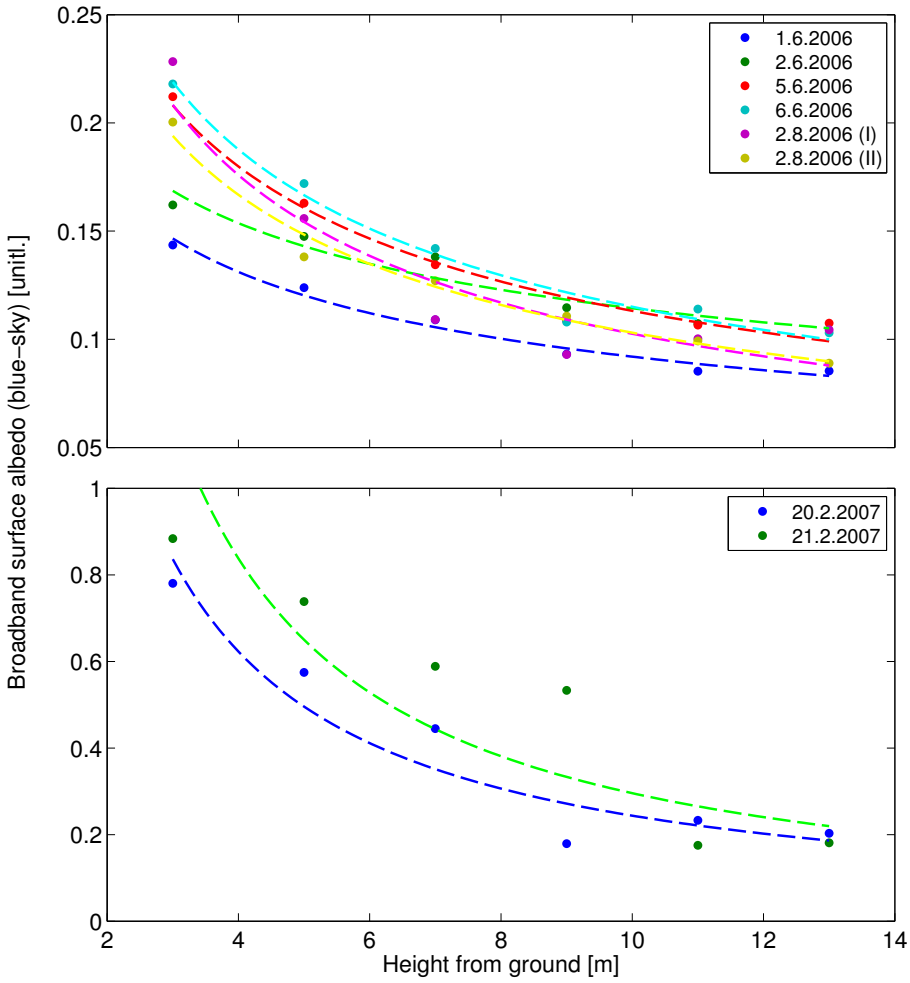

Figure 3.3: A summary of measured vertical albedo profiles for a Scots pine forest stand at FMI-ARC in Sodankylä, Finland. The forest stand was roughly 12 meters high. Upper subplot: Measurements from summer 2006, taken in cloud conditions with diffuse illumination. Lower subplot: Measurements from winter 2007, taken in clear-sky conditions with substantial snow cover on trees.

unidirectional. Yet, validation of such an albedo product using in situ pyranometer measurements raises an additional question of comparability; considering that atmospheric scattering and absorption alter the spectral irradiance measurable at Earth's surface compared to the TOA irradiance, is it justifiable to use ground-level pyranometer data (measuring blue-sky albedo which has a diffuse radiation component) to validate black-sky albedo products?

This question was explored in **Paper 4**. The theoretical difference between blue-sky and black-sky albedo was simulated using the SPCTRAL2 radiative transfer model (Bird & Riordan 1986) for a wide variety of natural surface types, Sun Zenith Angles (SZA) and atmospheric conditions, characterized by the Aerosol Optical Depth (AOD) at two wavelengths, as well as ozone and water vapour concentrations. The simulation results, consisting of over 200 000 individual cases, were then exploited to construct an empirical regression equation which allows the estimation of black-sky albedo from actual blue-sky albedo measurement data. Finally, the regression equation was tested on measurements from the Cabauw Baseline Surface Radiation Network (BSRN) station in the Netherlands (Knap 2012).

The simulation results showed that the relative blue-sky/black-sky differences are typically on the order of 5-10%, although differences of more than 20% can occur with large AOD or SZA values. The contributions of ozone or water vapour were slight. Surface type plays a role, since the shape of spectral albedo as a function of wavelength can be very different (e.g. between water and grass) and aerosol scattering in the near-infrared wavelengths is less effective than in the visible, as mentioned in Section 3.1. The difference is weakly dependent on SZA up to about 60 degrees, above which the difference increases strongly as a result of large atmospheric path lengths.

The simulated radiative fluxes contained both the direct and diffuse component, therefore an empirical regression relating the blue-sky albedo to the black-sky albedo through the radiant flux densities, AOD at 440 and 870 nm wavelengths, and SZA was sought. The regression was intentionally formulated as $\alpha_{BSA} = \alpha_{blue-sky}(1 + \dots)$ to follow convention and the individual term expression were formulated to resemble the diffuse radiation formulation terms in the model by Bird & Riordan

(1986). The resulting relationship was

$$\begin{aligned}\alpha_{BSA} = \alpha_{blue-sky}\big[c_0 + c_1\frac{1-exp(-\tau_{440}/cos\theta_s)}{1-\alpha_{blue-sky}} \\ + c_2\frac{1-exp(-\tau_{870}/cos\theta_s)}{cos\theta_s} \\ + c_3\frac{I_{dir}/1367(1-exp(-\tau_{440}/cos\theta_s))}{cos\theta_s^2} + c_4 I_{diff}/1367\big]\end{aligned} \tag{3.2}$$

where the parameters are as listed in Table 3.1 below.

Table 3.1: Listing of terms in Equation 3.2

α_{BSA}	Black-sky albedo
$\alpha_{blue-sky}$	Blue-sky albedo
τ_{440}	Aerosol Optical Depth at 440 nm
θ_s	Sun Zenith Angle
τ_{870}	Aerosol Optical Depth at 870 nm
I_{dir}	Direct radiant flux density
I_{diff}	Diffuse radiant flux density
$c_0 \ldots c_4$	numerical regression parameters (Table 2 of **Paper 4**)

It should be noted that since the albedo of snow and ice has a large range of variability (Warren & Wiscombe 1980), our small sampling of snow spectra is not expected to produce a regression equation valid for all snow and ice conditions. The accuracy of Equation 3.2 was calculated in **Paper 4** to be quite good, the 90% relative error quantile being approximately 8% (relative). Large Sun Zenith Angles of over 60 degrees can cause larger estimation errors.

In addition to Equation 3.2, another regression equation in similar form was introduced for cases where AOD data is not available. In this case, the black-sky albedo is estimated from blue-sky albedo using solely the direct and diffuse radiative flux densities and SZA. This alternative regression generally works almost as well as the full regression, although at long atmospheric path lengths (i.e. large SZA) its performance decreases notably.

Testing the regression to measurements from BSRN Cabauw site showed that typical differences between blue-sky and black-sky albedo are up to 5% (relative). The magnitude of the difference is similar to that proposed previously by Key et al. (2001). Considering that the data from Cabauw exhibits a large range of atmospheric conditions, it seems therefore safe to conclude that using blue-sky ground albedo measurements (from non-cloudy periods) to validate black-sky albedo products is justifiable over most atmospheric conditions, with the exception of very large SZAs. As discussed in section 2.4, SAL discards all observations where SZA exceeds 70 degrees, thus avoiding the most inappropriate comparison cases.

3.4 Validating SAL over the Arctic

In this section, I will summarize the observed performance of the SAL products over the Arctic. The emphasis shall be on the 28-year CLARA-A1-SAL dataset, whose data will be utilized in Chapter 4 to assess the trends in Arctic sea ice albedo. The results summarized here are from **Papers 1** and **2**.

Perennial snow

The retrieval capabilities of CLARA-A1-SAL for (perennial) snow were assessed at five perennial snow validation sites; three of which were on the Greenland Ice Sheet and two on Antarctica. The Antarctic site results are included here for completeness, although our focus is on the analysis for the Arctic sites. The site locations are illustrated in Figure 3.4. The full site names are listed in Table 3.2.

Validation of satellite albedo retrievals with in situ data requires that the data be matched temporally, spatially (at least assessing site representativeness as in Section 3.1), and spectrally. In my analysis, the in situ observations and SAL data were matched temporally by recording the successful retrieval timestamps in CLARA-A1-SAL at each site, and subsequently selecting only corresponding ground observations for comparison. This allowed me to exclude cloudy-sky in situ observations, in which snow albedo is typically 0.05 to 0.1 higher than for clear-sky conditions (Key et al. 2001). Spatial representativeness for perennial

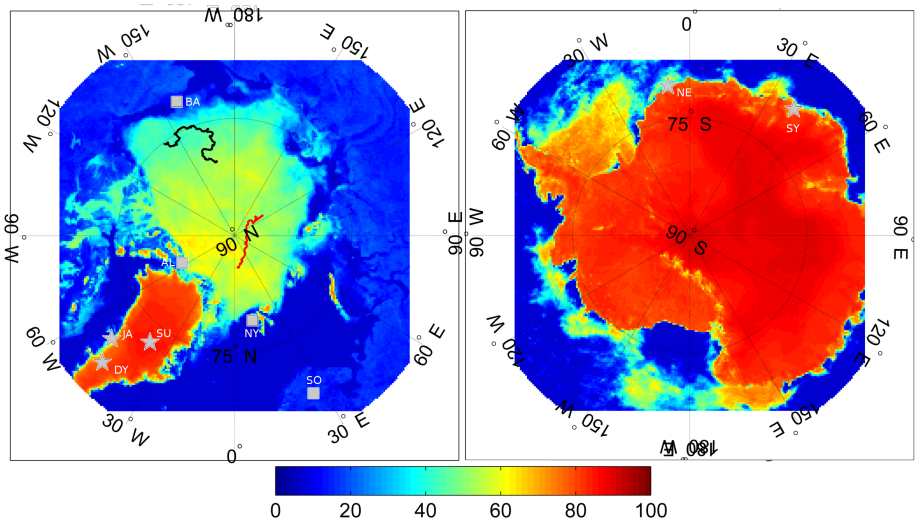

Figure 3.4: Locations of the CLARA-A1-SAL validation sites over the Arctic and Antarctic. Gray stars indicate perennial snow sites, gray squares indicate seasonal snow sites. The black line shows the SHEBA floating ice camp locations in 1997, and the red line shows the Tara floating ice camp locations in 2007. The locations are overlaid on CLARA-A1-SAL monthly mean products from July 2009 (Arctic) and January 2009 (Antarctic)

snow sites is not an issue, as mentioned earlier in section 3.1. Spectral matching of the in situ data to the broadband SAL products was also considered (**Paper 2**). Excluding the DYE-2 and JAR-2 sites on GrIS, the pyranometers used were capable of observing the full broadband albedo, requiring no matching operations. The LI-COR200SZ pyranometers at the two sites had limited sensitivity (0.4 - 1.1 μm), which leads to a reported bias of 0.04, or roughly 5-6% relative (Stroeve et al. 1997). In my analysis, this bias was simply considered as a part of the in situ data uncertainty.

While the initial validation of SAL snow albedo was limited to a single year (2007) in **Paper 1**, the 28-year coverage in CLARA-A1-SAL enabled me to extend the validation period significantly. Between 9 and 15 data-years were processed for each site. The validation metrics

were also expanded, showing seasonal mean differences between SAL and in situ data in addition to the conventional RMSE values. This gives better insight to any seasonally varying effects in SAL retrieval quality.

The validation results are summarized in Table 3.2. CLARA-A1-SAL albedo retrievals of continuous snow fields are fairly good, with relative accuracy typically around 5% relative. The good agreement is partly due to negligible site representativeness issues on perennial snow fields and the AVHRR radiance intercalibration to MODIS and in situ standards, but it also validates the chosen retrieval approach as discussed in section 2.4. Also, the limitations in CLARA-SAL atmospheric correction - the fixed AOD and ozone content - do not have a large impact over the Arctic. Previous studies propose that typical AOD over the Greenland Ice Sheet is in the range of 0.05 - 0.1, and thus well-matched to the CLARA-SAL AOD level. The effect of ozone variations is limited in comparison to aerosols, as mentioned in section 2.4.

The retrieval accuracy is similar to that shown previously for the APP-X dataset by e.g. Stroeve et al. (1997), Stroeve (2001). The DYE-2 and Summit sites are high on the GrIS and have in the past typically experienced little or no surface melt, leading to a stable albedo year-round. The JAR-2 site, located in the ablation region of the ice sheet, experiences far more seasonal albedo variation as a result of surface melt and influx of dust from the Greenland coast, as also reported by Stroeve et al. (1997). This implies more challenging retrieval conditions for CLARA-A1-SAL, which is seen as larger scatter in retrieved albedo vs. in-situ observations (see Figure 3.5 for the retrieved CLARA-A1-SAL albedos at JAR-2 in 2005).

It should be noted here that Box et al. (2012) have reported a decrease in snow albedo over the central parts of GrIS in the 2000s based on MODIS snow albedo retrievals. However, CLARA-A1-SAL has not detected an appreciable decrease over the Summit site, which is situated in the middle of the ice sheet (Figure 3.6 shows the full CLARA-A1-SAL timeseries over the area). Given that AVHRR is, even after the radiance intercalibration, a less sensitive instrument than MODIS, it is possible that the albedo decrease over central GrIS has not been large enough to be detectable by AVHRR, or that the arguably more precise atmospheric correction in MODIS enhances its detection capabilities for less dramatic trends. Quantification of differences in atmospheric cor-

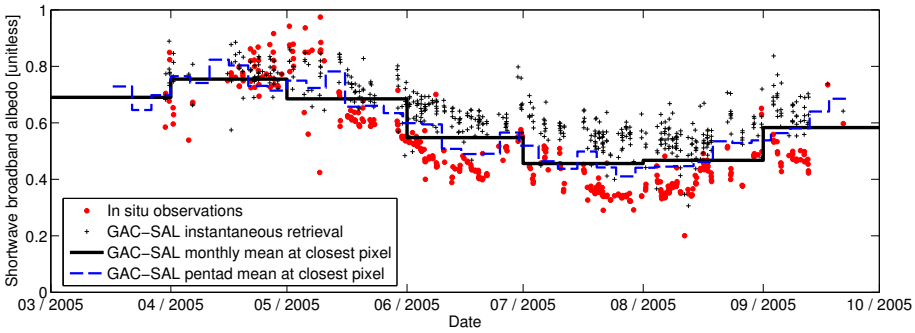

Figure 3.5: Example of validation results of CLARA-A1-SAL at the JAR-2 site, in the ablation region of the Greenland Ice Sheet. The year shown is 2005.

rection accuracy is a challenging task and not within the scope of this dissertation. This question remains open for future study at this time.

Table 3.2: The CLARA-A1-SAL validation results for (perennial) snow and ice sites. The seasonal abbreviations are: DJF = December-February, MAM = March-May, JJA = June-August, SON = September-November.

Site	Latitude [deg N]	Longitude [deg E]	Period	Pentad RMSE	Monthly RMSE	seasonal (mean) relative retr. error [%] DJF	MAM	JJA	SON
DYE-2 (DY), GrIS	66.48	-46.28	1996-2009	0.041	0.036	-	+1.40	+2.17	-0.71
JAR-2 (JA), GrIS	69.42	-50.06	1999-2007,2009	0.082	0.064	-	+5.34	+7.68	+6.01
Summit (SU), GrIS	72.58	-38.50	1995-2005,2007-2009	0.062	0.042	-	+4.37	+2.54	-0.20
Neumayer (NE), Antarctica	-70.65	-8.25	1995-2009	0.174	0.173	-13.52	-17.92	-	-8.56
Syowa (SY), Antarctica	-69.00	39.59	1998-2009	0.175	0.188	-2.85	-2.68	.	-13.88
SHEBA, Arctic Ocean	variable	variable	1998	0.081	-	-	-	-	-
Tara, Arctic Ocean	variable	variable	2007	0.090	-	-	-	-	-

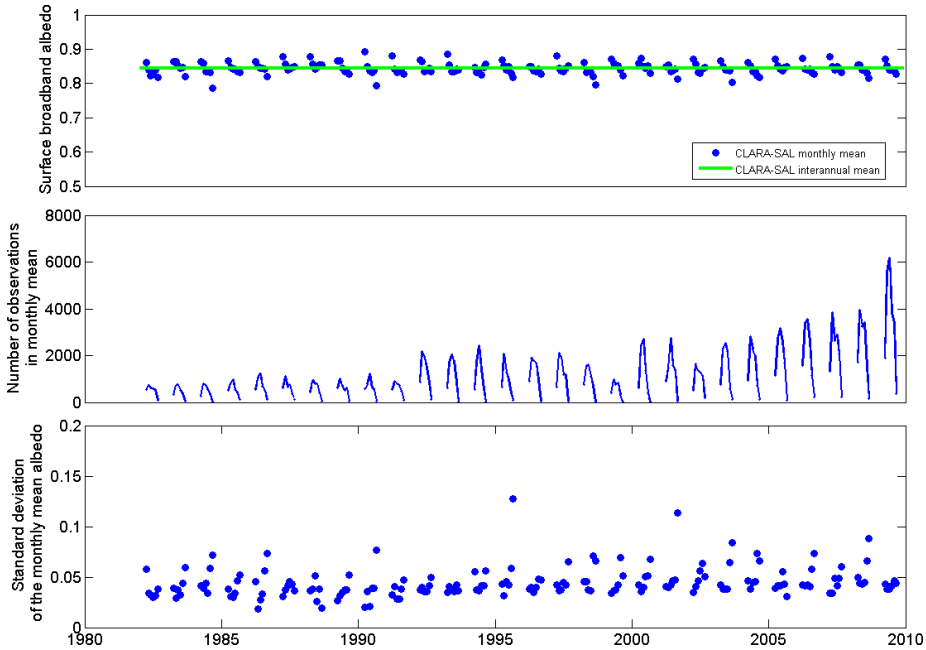

Figure 3.6: Upper subplot: A 1982-2009 timeseries plot of monthly mean CLARA-A1-SAL albedo retrievals of the grid cell containing Summit camp, near the top of the Greenland Ice Sheet. Middle subplot: number of observations used in the monthly mean calculation. Lower subplot: Standard deviation of the monthly mean albedo.

We have focused on validation results for CLARA-A1-SAL thus far, but also the validation carried out for the operational Arctic SAL product in **Paper 1** produced very similar results. This is understandable given that the retrievals followed similar logic, excepting somewhat different product averaging, the presence of a radiance intercalibration in CLARA-A1-SAL and the omission of the SZA normalization routine in CLARA-A1-SAL. The radiance intercalibration had a small effect on the most recent AVHRR instruments (Heidinger et al. 2010), so that the AVHRR input radiance data for the study in **Paper 1** should resemble CLARA-A1-SAL data quite well. The averaging differences are not significant (resolution changed from 15 to 25 km^2, and time resolution from weekly to pentad), and the effect of the omitted SZA normalization to 60

degrees is small over the Polar regions, where SZA input varies naturally between 50 and 70 degrees (SAL cut-off) over the polar summer.

As a final note, the validation results from the Antarctic sites (Table 3.2) are similar to those from GrIS sites. The higher RMS error results mainly from the coastal location of the Antarctic sites; the 25 kilometer CLARA-SAL grid cell containing the site is composed of a varying mixture of snow, ice and open water which causes the larger difference.

Arctic sea ice

Validation of CLARA-A1-SAL for the Arctic sea ice presents a problem of in situ data scarcity. Over the last three decades, quality-controlled in situ measurements of sea ice albedo over a full melting season have (to my knowledge) only been carried out on two expeditions: the Surface Heat Budget of the Arctic Ocean (SHEBA) field campaign between 1997 and 1998 (Perovich et al. 2002), and the Tara expedition between 2006 and 2008 (Gascard et al. 2008). Both expeditions were actually floating ice camps, carried on the sea ice around the Arctic sea ice zone. The drifts of the ice camps are shown in Figure 3.4. Tara measurement point was fixed and measurements continuous, SHEBA measurements took place every 2.5 m along a 200-meter long line on every other day during summer (June-August).

The drift of the ice camps poses an additional challenge to the validation, as the in situ measurement location is variable. This was accounted for in the validation study by selecting the CLARA-SAL grid cell closest to the respective ice camp locations as the applicable satellite retrieval. Sea ice as a material also potentially poses a representativeness problem; ground truth albedo measurements may not correctly represent the fraction of open water leads and/or melt pond coverage, both of which have a large impact on the areally integrated sea ice albedo as a result of the large reflectivity contrast between ice and water (Grenfell & Maykut 1977, e.g). Fortunately, sea ice albedo was measured from a C-130 aircraft during the SHEBA campaign, the results being in agreement with the ground truth observations although the aircraft measurements covered a somewhat larger area (Curry et al. 2001). Based on these results, I found no reason to question the areal representativeness of the SHEBA albedo data.

As previously discussed in the Subsection on perennial snow validation, cloudy-sky in situ albedo observations have been excluded from the analysis. However, owing to the persistent cloudiness over the Arctic Ocean (Key et al. 2001), exclusion of all cloudy-sky albedo data from the field campaigns would render the reference dataset too small to draw any conclusion on CLARA-SAL performance. Therefore, the sea ice reference albedo was calculated as a mean of all in situ observations in the validation timeperiod for which SZA is less than 70 degrees. Snow albedo is typically 0.05 higher under clouds (Key et al. 2001). The magnitude of this effect actually changes during the polar summer, because the progressing surface melt increases the size and frequency of melt ponds on the sea ice, and the albedo of these ponds depends much less on cloudiness. Late-season melt pond drainage will again expose bare ice and increase the cloudiness effect somewhat. Owing to this complex interplay of surface conditions and clouds, I have chosen to consider the in situ data to have an uncertainty of 0.05 in lieu of attempting a correction, which could potentially induce an artificial bias in the results depending on melt season characteristics.

The validation results against both SHEBA and Tara campaign data are shown in Figure 3.7 and listed in Table 3.2. The results are broadly similar for both campaigns, showing that CLARA-A1-SAL can retrieve the sea ice albedo with a fairly good degree of accuracy (5-15%), and that the satellite retrievals can track the evolution of sea ice albedo throughout the melting season. Outliers naturally occur, given that the low Sun elevation in August causes uncertainty in both the cloud detection (i.e. more misclassifications) in the AVHRR processing and in the surface albedo retrievals themselves. Mean RMSE for the pentad CLARA-A1-SAL products against SHEBA data was 0.081 and 0.09 against Tara data. The achieved accuracy is comparable to that reported for APP-X (0.07 albedo units by Key et al. (2001).

Land surfaces

CLARA-A1-SAL was validated at 14 land surface sites worldwide, using 180+ (cumulative) years of in situ data; for brevity and consistency, I will focus here on two Arctic sites: Sodankylä in Finnish Lapland, and Barrow in Alaska. Full validation results over all sites are available in

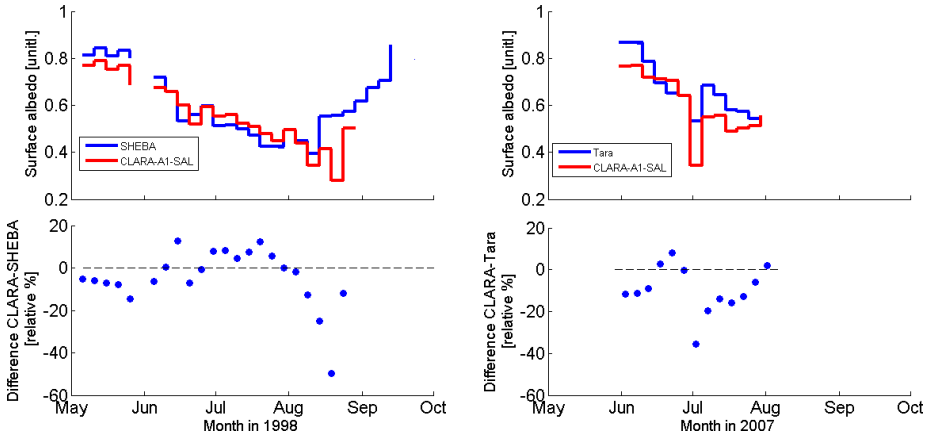

Figure 3.7: Upper subplots: CLARA-A1-SAL pentad mean albedos of the grid cell(s) over the floating ice camps versus the temporally averaged five-day mean in situ albedos. Lower subplots: Relative retrieval error of CLARA-A1-SAL versus in-situ data. Note that in situ data may have an uncertainty of up to 0.05 (see text for details).

Paper 2.

The Sodankylä site is maintained by the Arctic Research Center of FMI; the albedo measurements are taken from a 50-meter mast over a boreal forest stand. This mast is not the same as used in the measurements for **Paper 3**, although the shorter mast and its forest stand are within the field of view of the pyranometer used here. The quantitative site representativeness analysis discussed before suggested that the Sodankylä site is well representative of its surroundings during summer, although some caution is yet in order. While the reflectance characterics of the site and its surroundings are mostly similar in the summer analysis, the wetlands surrounding the research center likely have different diurnal and seasonal cycles in albedo compared to the boreal forests of the area. Thus, winter and the melting season can still exhibit different albedo cycles.

Figure 3.8 shows an example of the seasonal albedo cycle at Sodankylä for both in situ data and CLARA-SAL. The entire annual albedo cycle is not retrievable by CLARA-SAL due to solar illumination limitations. In the late winter and early spring, both in situ data and CLARA-

SAL mark the gradual decrease of the snow-covered surface albedo of the site as snow ages and begins to melt. CLARA-A1-SAL is negatively biased during this period. However, as previously stated, the albedo evolution of a potentially snow-covered boreal forest stand is different from the surrounding wetlands. Furthermore, the perennial snow albedo validation discussed in section 3.4 should show a notable bias if the algorithm itself were at fault. The atmospheric correction is also not to blame, since the reported AOD over Sodankylä is well-matched with SAL input (Toledano et al. 2012). Considering also that both in situ data and SAL show a similar decreasing albedo trend prior to the relatively abrupt final melt of the snow cover, it seems highly plausible that the algorithm is not the source of the discrepancy.

The reader may also note that the in situ winter albedo shown in Figure 3.8 is considerably higher than that measured just over the canopy (at 13 meters height) in **Paper 3**. There are several factors at work here. Firstly, the reference albedo measurements for the validation are made from a 50-m tall mast, meaning that the measured area at canopy level (12 m height) is more than 150 times larger compared to a measurement from 13 meters height. The terrain visible to the mast measurement of reflected radiation is therefore certainly different. It should also be noted that albedo measurements just over the canopy, while better representative of forest stand albedo than understory measurements, may still have a height-dependent component as tree stems and brances are likely more visible than higher above the canopy. As seen in Figure 3.8, the in situ albedo can also vary greatly over the spring depending on the presence of snow or frost on the trees (as also measured by Kuusinen et al. (2012) for a site in Southern Finland). Finally, tree density can also play a role in the typically sparse boreal forest, as the measurements in **Paper 3** were taken with the albedometer quite close to a patch of trees, whereas the validation reference measurements from the tall mast may see a different fraction of open, and thus certainly snow-covered, ground.

In contrast, we find that the summer CLARA-A1-SAL retrievals at Sodankylä are in very good agreement with the in situ reference. This is supported by the site representativeness analysis in **Paper 2**, which showed the Sodankylä site to be one of the most representative of its surroundings. This does not necessarily mean that the land cover is homogeneous, but it does imply that the reflectance characteristics of the

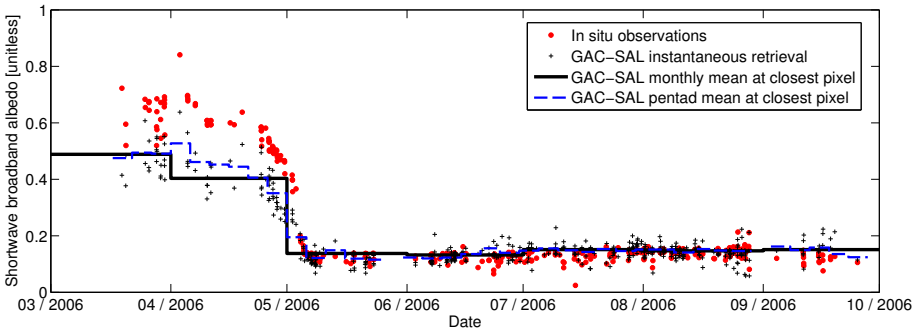

Figure 3.8: In situ albedo observations (red circles) versus CLARA-A1-SAL albedo retrievals at Sodankylä site in 2006. Black and blue (dashed) lines indicate monthly and pentad CLARA-A1-SAL means, respectively. Black crosses indicate instantaneous CLARA-A1-SAL retrievals at AVHRR-GAC resolution.

surrounding wetlands and forests are more similar in the summer.

At Barrow, the coastal location of the site and the numerous small-scale lakes and ponds create challenging conditions for surface albedo retrieval and validation at AVHRR-GAC resolution. This is well reflected in the representativeness analysis in **Paper 2**, where Barrow was ranked as one of the least representative sites at CLARA-A1-SAL scale.

Figure 3.9 illustrates the validation results obtained at Barrow. Underestimations of site albedo are common, which is typical for coastal sites where open water albedo tends to bias the 0.25 degree CLARA-A1-SAL averages low relative to in situ observations over land. Of special note in Figure 3.9 is that even the AVHRR GAC-resolution instantaneous retrievals (black crosses) at Barrow are often classified as occurring over open water, a definite signature of the coastal mixed-pixel problem. This issue cannot be easily resolved in coarse resolution imagery, which is why other studies have advocated the use of higher resolution imagery in analyzing shortwave radiation characteristics of coastal sites (Niu & Pinker 2011).

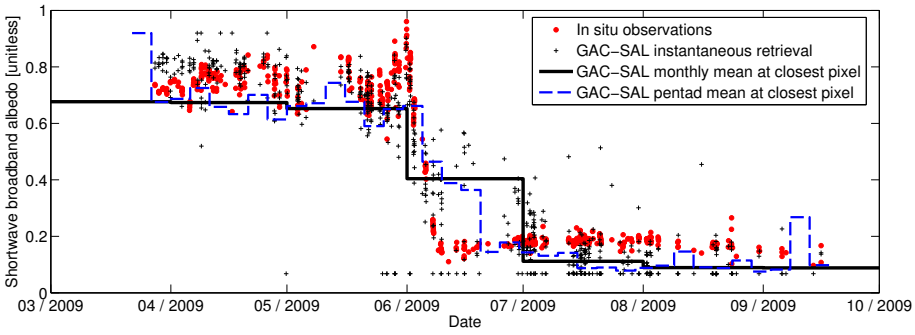

Figure 3.9: In situ albedo observations (red circles) versus CLARA-A1-SAL albedo retrievals at Barrow site in 2009. Black and blue (dashed) lines indicate monthly and pentad CLARA-A1-SAL means, respectively. Black crosses indicate instantaneous CLARA-A1-SAL retrievals at AVHRR-GAC resolution.

4 APPLICATION TO TRENDS IN ARCTIC SEA ICE ALBEDO

The Arctic sea ice has undergone considerable changes over the past decades. Beyond the well-documented retreat of the ice cover (Stroeve et al. 2007, Parkinson & Cavalieri 2008) and the related transformation of the remaining ice from thick multiyear ice into thin first-year ice (Maslanik et al. 2007, Kwok & Rothrock 2009), studies have also shown that the ice melt season is growing longer (Markus et al. 2009) and the ice is moving faster (Rampal et al. 2009). Considering all this, the assessment of Arctic sea ice albedo trends is a topical study and an appropriate first use of the CLARA-A1-SAL dataset created during this dissertation work. By following the prerequisite retrieval and validation work with an application of the dataset for climate monitoring purposes, it is also the culmination and final study of this dissertation (**Paper 5**).

The CLARA-A1-SAL validation in **Paper 2** showed that sea ice albedo can be retrieved with a satisfactory level of accuracy and that AVHRR intercalibration issues have largely been resolved with the radiance homogenization. Therefore, the dataset should be reliable enough for sea ice trend analysis. To further diminish the effects of retrieval uncertainties in the trends, I decided to focus on the mean albedo trends over the Arctic Ocean. Robust AVHRR-based retrievals over the entire Arctic Ocean are possible during the melt season (May to August), which is, fortunately, also the most interesting period for the albedo dynamics. Keeping to the large-scale study philosophy, I also decided to only study the monthly means. Maximizing the number of independent overpasses per analyzed product also helps with minimizing effects of retrieval errors according to the law of large numbers.

As a further quality control measure, I discarded any SAL grid cells

where the montly mean albedo was derived from fewer than 60 AVHRR overpasses. The threshold was empirically chosen to remove nearly all of the obviously poor-quality retrieval areas near the North Pole in August, where the low Sun elevation limits data availability and causes cloud misclassification errors. This thresholding typically creates a variably large no-data area in August over the North Pole. This changing no-data area could conceivably bias the mean Arctic Ocean albedo for August and obfuscate its trend. To prevent that, I implemented a gap-filling algorithm (Garcia 2010) which not only considered the albedo of the surrounding sea ice, but also the albedo of the region during June and July for each year. This "memory" of sea ice conditions should help in keeping the gap-filled albedo estimates realistic. For completeness, I analyzed both original and gap-filled data and compared the results.

The CLARA-A1-SAL dataset was processed for trend calculation using two masking operations. In the first one, I excluded all land surfaces using the Global Self-Consistent Hierarchical High-Resolution Shoreline data as a mask (Wessel & Smith 1996). Averaging the remaining grid cells provides the mean albedo of the composite of open water and sea ice. Examining the means month per month through the 28 years of coverage is expected to produce a negative albedo trend, considering the a priori knowledge of sea ice retreat and the presence of a negative albedo trend in the AVHRR-based Extended Polar Pathfinder dataset (Wang & Overland 2012).

By further masking out open water areas using the NSIDC/NASA Team microwave-based sea ice concentration data (Cavalieri et al. 1996), it is possible to exclusively study the mean albedo of the sea ice zone (defined as the area where ice concentrations area above 15%). The relative size of the sea ice zone is between 35 and 85% of the composite open water-sea ice study area, depending on month and year. If each month is studied separately, then the insolation may be considered similar across the monthly samples and the resulting trends thus reveal changes in the mean surface conditions of the sea ice. Keeping in mind that SAL is a black-sky albedo product and assuming that cloud masking is accurate, any changes or trends in cloudiness only affect the amount of available data for each monthly mean albedo. The accuracy of cloud masking has been evaluated to be approximately 90% during the Arctic summer (Karlsson & Dybbroe 2010), which I consider sufficient to ensure that

the remaining misclassfied clouds do not have a noticeable impact on the Arctic Ocean-wide average albedo. Using microwave-based ice concentration to identify ice coverage is also more reliable than thresholding using optically retrieved albedo alone. Figure 4.1 illustrates the correspondence of sea ice concentration against retrieved sea ice albedo in August over the full period 1982-2009 and over all of the Arctic sea ice zone.

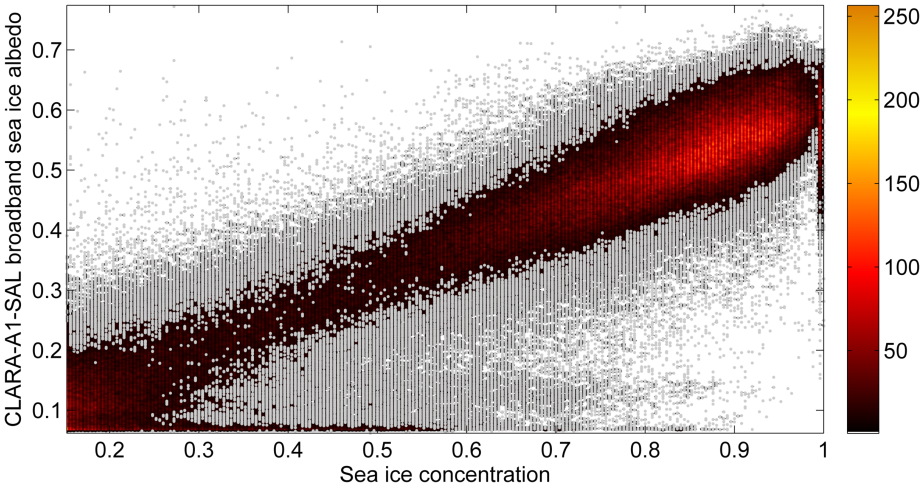

Figure 4.1: Density scatterplot of retrieved 0.25 degree CLARA-A1-SAL estimates (y-axis) versus nearest-neighbor NSIDC/NASA team retrieved sea ice concentrations (x-axis). Plot shows all retrievals over the Arctic sea ice zone in August for the years 1982-2009.

The composite albedo means across the CLARA-A1-SAL dataset are shown in the upper subplot of Figure 4.2, and the means for sea ice albedo alone in the lower subplot. As expected, the composite albedo trends reflect the sea ice retreat through a (statistically significant) negative trend for all months. The strength of the negative trend (Table 4.1) increases as the melt season progresses, as was expected given the increasingly positive late-summer temperature anomalies (Serreze et al. 2009) across the Arctic as well as the lengthening melting season (Markus et al. 2009).

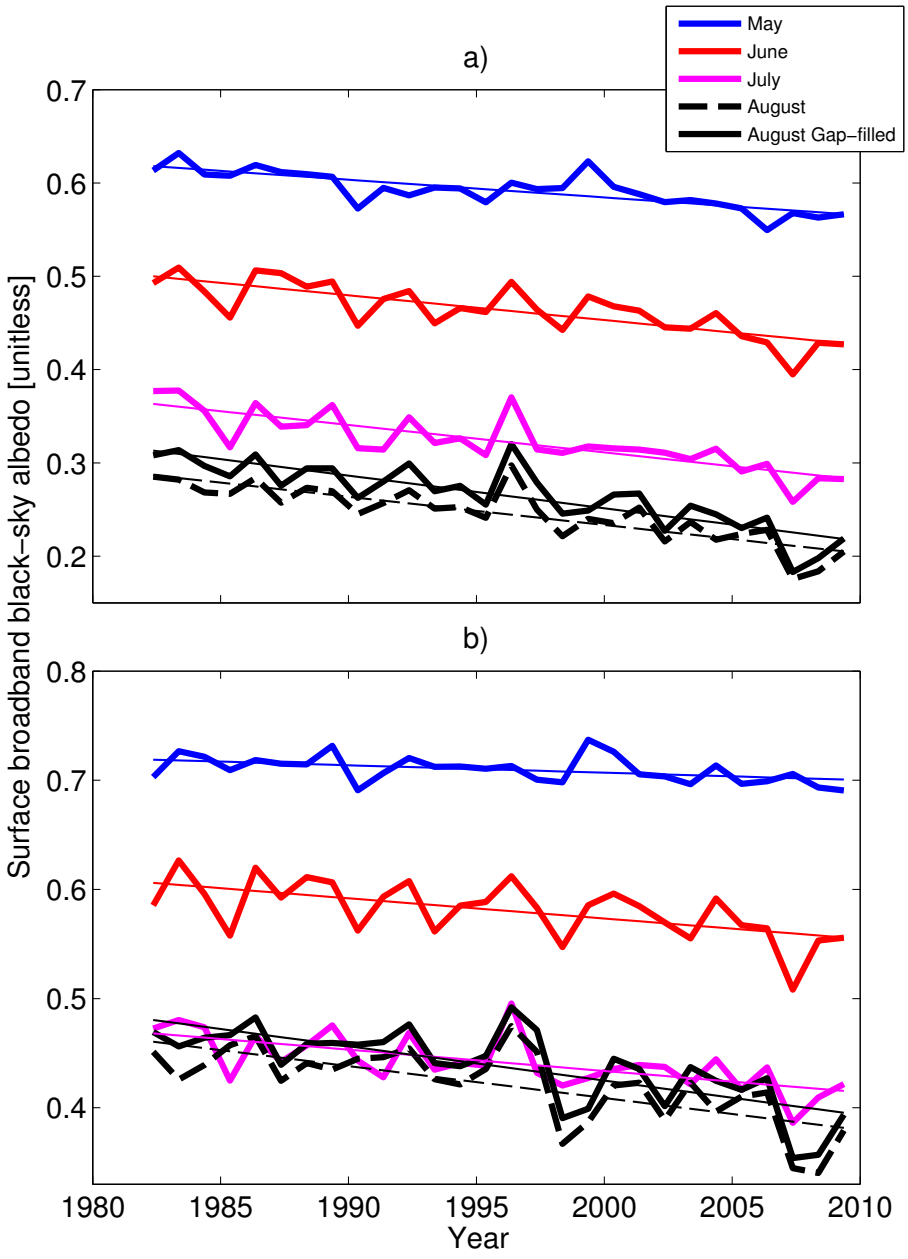

Figure 4.2: Upper subplot: Changes in the mean open water-sea ice composite albedo of the Arctic between 1982-2009. Lower subplot: Changes in the mean sea ice zone albedo of the Arctic between 1982-2009. Thin solid lines indicate best-fit linear trends. Dashed lines indicate non-gapfilled August data.

Table 4.1: Observed trends in monthly mean albedos through least-squares fitting. GF means gap-filled data. Trend uncertainties calculated at the 95% confidence interval.

Month	linear trend slope (units/decade)	R^2
May, composite	-0.019 $\pm$ 0.006	0.62
May, sea ice	-0.007 $\pm$ 0.005	0.21
June, composite	-0.027 $\pm$ 0.009	0.61
June, sea ice	-0.019 $\pm$ 0.010	0.35
July, composite	-0.029 $\pm$ 0.008	0.66
July, sea ice	-0.020 $\pm$ 0.009	0.44
August, composite	-0.030 $\pm$ 0.008	0.70
August, sea ice	-0.029 $\pm$ 0.011	0.50
August GF, composite	-0.035 $\pm$ 0.009	0.70
August GF, sea ice	-0.032 $\pm$ 0.012	0.54
August GF & denoised, sea ice	-0.032 $\pm$ 0.006	0.82
Month	2nd degree polynomial (x=years since 1982)	R^2
August GF, sea ice	$-0.0002x^2 + 0.0015x + 0.461$	0.61
August GF & denoised, sea ice	$-0.0002x^2 + 0.0020x + 0.458$	0.95

The sea ice zone albedo means show similar negative trends. This finding is perhaps not intuitively clear; it could be assumed that the summer melt as well as warm air and ocean currents would affect the marginal sea ice much more strongly than the sea ice of the central Arctic Ocean, keeping the sea ice albedo of the ice-masked region high after the lowest ice concentrations are discarded. According to the data this is not so. The albedo of the central Arctic, home to much of the oldest and thickest multiyear ice, is also decreasing. This implies that average surface conditions of the sea ice have been changing throughout the Arctic over the past three decades. The late-summer mean ice albedo has decreased the most (Table 4.1). This can be expected given the increased solar heat input from longer melting seasons (Markus et al. 2009, Perovich & Polashenski 2012).

An interesting question relating to the albedo decrease is whether it has been going on for the entire duration of the data coverage. Laine (2004) analyzed the Arctic sea ice albedo from the APP-X dataset be-

tween 1982-1998 and found only small or negligible negative trends in the sea ice albedo. To compare results, we repeated the analysis of the CLARA-A1-SAL dataset for the same period. The subset trends agreed with the results of Laine within the uncertainty limits. The subset trends particularly for the late summer were substantially weaker than the full period trends. This is an indication that the mean surface conditions may have changed more rapidly in the 2000s than before, particularly for the late summer period. However, there is considerable variability in albedo means of the sea ice zone, particularly in August. E.g. West et al. (2013) states that for two trend slopes to be considered different in the statistical sense, the trend slope uncertainties must not overlap. This condition is not fulfilled for neither the 1982-1998 subset nor the full period sea ice albedo trends in CLARA-A1-SAL. Therefore, the possibility that the apparent acceleration of albedo decrease is illusory must be acknowledged.

The trend uncertainties in general were calculated at the 95% confidence interval using the two-tailed t distribution critical value and the standard error of the regression slope. As mentioned, the late-summer monthly means have the largest variability and therefore the largest trend uncertainties. Yet, it remains clear that there is a negative trend in mean sea ice albedo for all months except May.

Considering the albedo decrease, one is next tempted to ask what causes it. I sought to answer this question for the sea ice zone albedo by considering the likely physical drivers of albedo change. If we consider sea ice albedo in an areally integrated sense, then sea ice concentration must be a strong driver of albedo because of the large albedo contrast between open water and sea ice, even if it is bare ice (Perovich et al. 2007). The other significant driver must be the (mean) surface condition of the ice - is it snow-covered or not, is the snow fresh or old, are there melt ponds, and if yes, how large and deep are they? Following this logic, I chose mean surface air temperature (SAT) of all regions North of 65 degrees of latitude, and the mean length of the melting season to-date (day of year minus melt onset date) as the other inputs for a multiple linear regression of the observed mean sea ice zone albedo. I chose linear regression because the relationships should be linear in nature - areally integrated sea ice albedo is a linear function of ice concentration, the energy transfer from air to sea ice is a linear function of the near-surface

air temperature, and the phase changes in sea ice surface accumulate linearly according to the length of the experienced melt season.

The ice concentration data was extracted from the the NSIDC NASA Team passive microwave sea ice concentrations product (Cavalieri et al. 1996), SAT data from the NCEP-DOE AMIP-II reanalysis (Kanamitsu et al. 2002), and melt onset dates from the dataset by Markus et al. (2009). All data sets were spatially averaged; ice concentration was averaged over the area commonly agreed to be the sea ice zone (concentrations above 15%), SAT was averaged over all regions North of 65 degrees latitude, and melt onset date was calculated as a single average melt onset date (per year) over the full sea ice zone.

The proposed multiple linear regression turned out to be very capable of explaining the variability in the mean sea ice zone albedo, as shown in Figure 4.3. The negative trends are tracked, as is most of the year-to-year variability. This result is of course expected given the previously discussed theory, but obtaining such a good agreement between data from independent instruments (optical and microwave-based) and SAT reanalysis reinforces the robustness of the observed albedo and its trend.

The equation for the best-fit multiple linear regression is

$$\alpha_{SI} = 0.6387 * C - 0.0065 * SAT_{65-90N} - 0.0011 * (DOY - MOD) + 0.0676 \tag{4.1}$$

where C is the average sea ice concentration over the Arctic, SAT_{65-90N} is the average SAT of all regions north of 65N, DOY is the average day of year of each monthly mean (15th day of month), and MOD is the average day on which onset of melt occurred over the Arctic. The constant term was forced as 0.0676 to ensure that the parameterization agrees well with open water albedo when C is zero (at a Sun Zenith Angle of 60 degrees).

The scope and range of the parameterization is limited; it considers only averaged variables over the entire Arctic sea-ice zone, its temporal validity is limited to the melting season and, being empirical in nature, has limits on the validity range of SAT. Passive microwave-based ice concentrations are generally biased low during the melt season, also contributing to the bias of the parameterization (Fetterer & Untersteiner 1998).

The relative contribution of the albedo drivers in Equation 4.1 for August is visualized in Figure 4.4. The negative albedo trend is mainly

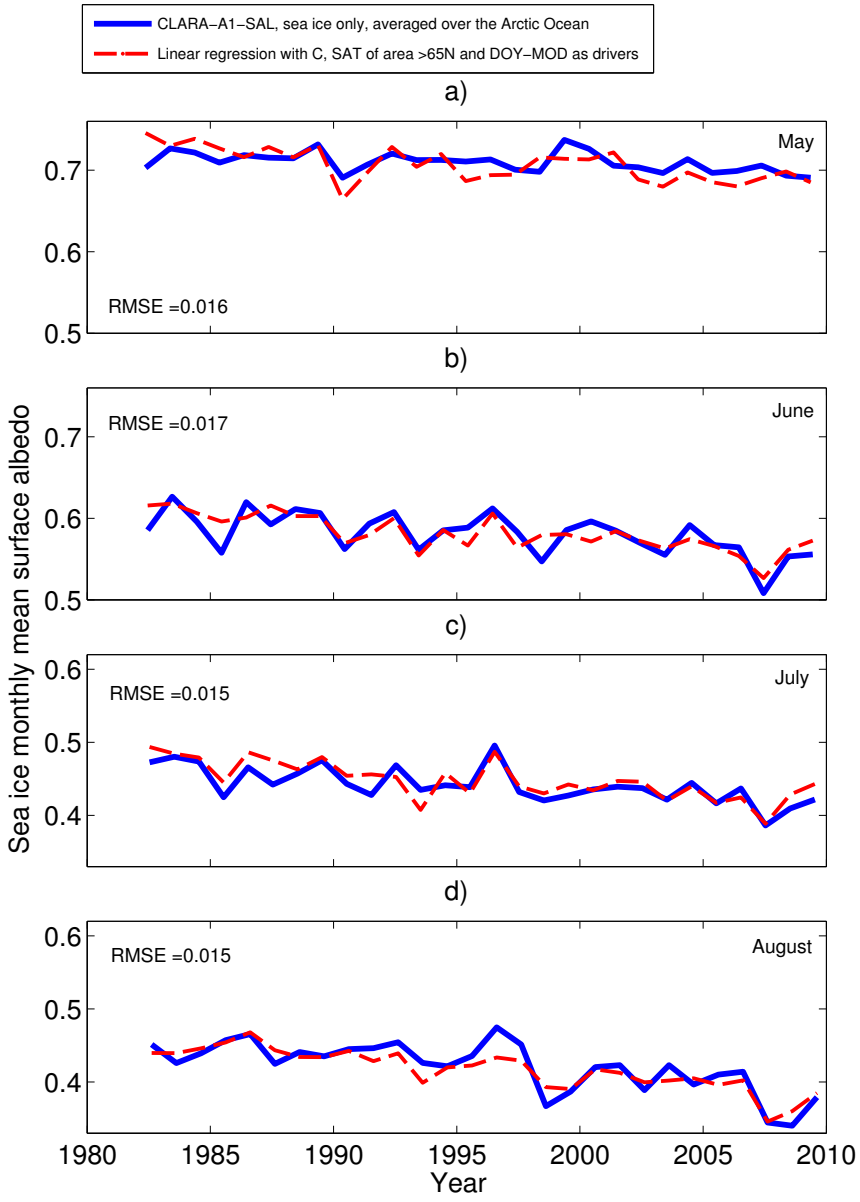

Figure 4.3: CLARA-A1-SAL monthly mean Arctic sea ice zone albedo (blue line) and the parameterized sea ice zone albedo using ice concentration, SAT and time since melt onset as drivers. All albedo and driver data are averaged over the entire Arctic sea ice zone.

caused by a diminishing mean sea ice concentration and an increase in SAT. The melt season length term varies only slightly in comparison. The static open water albedo term is not plotted for clarity.

On the other hand, it should be acknowledged that the drivers used are not fully independent from each other. Large increases in SAT or melt season length will cause a reduction in sea ice concentration due to melting. Also, an increasing sea ice concentration affects the atmospheric dynamics of the sea ice zone, potentially reducing SAT and inhibiting melt through the albedo feebacks on the surface radiative budget. It should therefore be considered likely that further study of sea ice albedo parameterization based, for example, on CLARA-A1-SAL could yield an improved parameterization equation where the drivers have a greater degree of independence from each other.

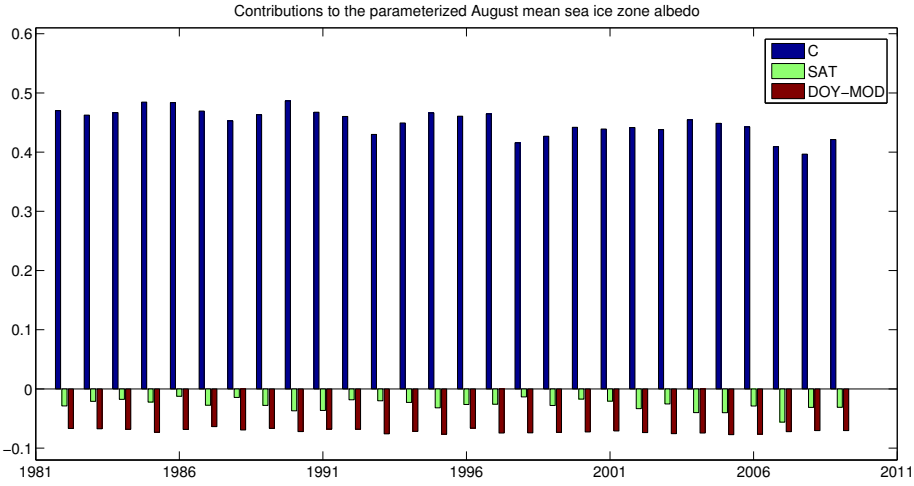

Figure 4.4: Contributions of the three drivers to the mean sea ice zone albedo (non-gapfilled for August).

The observed sea ice albedo from CLARA-A1-SAL is consistent with field study results, implying a relatively low bias in the retrievals. The albedo trends agree well with independently derived estimates of changes in the main drivers of sea ice albedo. The albedo retrievals naturally have an associated uncertainty, which is admittedly largest for the late summer season when the largest changes have been observed. Yet,

the albedo data fits very well with sea ice concentration and SAT data, which have been derived with means that are independent from optical satellite measurements and do not share error sources. Considering this, I find it very likely that the observed trends are real and that their attribution, as shown above, is justified.

5 | CONCLUSIONS

This dissertation has sought to increase our understanding of the remote sensing of snow albedo in the Arctic regions. The main satellite dataset has come from the AVHRR family of instruments, spanning 1982-2009. In situ observations of surface albedo have been gathered from a variety of sources including floating ice camps, the BSRN observation network and my own field work. Therefore, a large dataset of in-situ observations has been available to validate the satellite retrievals made in this dissertation. Issues such as site representativeness and imperfect atmospheric effect compensation create a bias in the satellite retrievals and uncertainty in their validation accuracy. Overall, the satellite retrievals have been shown to be consistent and capable of tracking actual albedo changes in the snow and ice.

The main contributions of this dissertation are the following:

1. The SAL algorithm which retrieves surface albedo from AVHRR observations was implemented into operational use and validated (**Paper 1**). The algorithm was then reused in the processing of the 28-year CLARA-A1-SAL dataset, which was also thoroughly validated and compared with other satellite data (**Paper 2**).

2. The validation results showed that polar region albedo could be retrieved with an accuracy that is sufficiently good for climate monitoring applications (**Paper 2**). Thanks to the radiance intercalibration, the stability of the dataset was confirmed to be also sufficiently good for surface albedo trend studies (for the polar regions).

3. A semivariogram-based method was presented in **Paper 2** to quantify the comparability of coarse-scale satellite observations versus

a point-like ground measurement. This enabled the quality assessment of the validation results over sites on vegetated terrain.

4. Validation data on surface albedo is easiest to gather with pyranometers at ground level, but over forested sites this creates a discrepancy with the satellite observations, which mostly see the canopy level albedo signature of the site. **Paper 3** detailed an experimental study on the relationship between pyranometer observation height and boreal forest stand albedo. The relationship over summer under cloudy skies was found to follow a power law. The winter results were more ambiguous due to the effect of snow on the tree branches, as well as challenging illumination conditions.

5. Black-sky surface albedo products such as SAL are commonly validated using ground truth data from pyranometers, which measure the albedo in ambient conditions, i.e. with an atmospheric effect included. **Paper 4** was a study on quantifying the magnitude of the atmospheric effect in the pyranometer data. It was shown that a priori knowledge of diffuse radiative flux density and AOD at two wavelengths is sufficient to calculate the atmospheric effect. Typical overestimations at Cabauw test site were found to be approximately 5% (relative), although substantially larger values can occur.

6. The developed and validated CLARA-A1-SAL dataset was applied to study the albedo trends in the Arctic sea ice between 1982-2009 in **Paper 5**. The findings were that the basin-scale surface albedo of the Arctic is decreasing for most summer months, mainly as a result of the ongoing retreat of the sea ice cover. However, the study also showed that the remaining sea ice zone albedo clearly shows a negative trend - the remaining sea ice is becoming darker. The cause of this trend was investigated and it was found that the changes can be explained using mean ice concentration, mean surface temperature over the Arctic and time elapsed since melt onset as drivers. These findings fitted previous study results logically, reinforcing confidence in the veracity of the satellite-derived trend estimates.

The obtained results should prove of value in the study of the Arctic climate. In particular, the 28-year dataset created within this dissertation was recently released for the scientific community and there remain several potential applications for it apart from the sea ice albedo trend study done in this work. Combined with datasets on irradiance and cloud properties over the Arctic, it is possible to calculate radiative forcing estimates which correspond to the observed albedo changes. If independent large-scale datasets on black carbon deposition over the Arctic become available, they could be compared to the albedo estimates presented here for verification. And, of course, the snow and ice albedo data presented has been shown to be of good accuracy and thus should be applicable to the verification of albedo parameterizations in climate models, an important motivator for this work.

As ever, there were also points which could be improved on in the future. There remains some room for improvement in the atmospheric correction, although the current limitations do not significantly affect Arctic snow and ice albedo retrievals. Also, further work towards an even better delineation of clouds, open water and sea ice can only serve to make the resulting albedo retrievals more precise. As more and more long-term satellite datasets on snow and ice are becoming available, combining different datasets and data from different satellite platforms has the potential to create more coherent datasets and thus enhance our understanding of the Arctic and polar regions in general.

References

Ambach, W. (1985), 'Characteristics of the heat balance of the greenland ice sheet for modelling', *Journal of Glaciology* **31**(107), 3–12.

Betts, A. K. & Ball, J. H. (1997), 'Albedo over the boreal forest', *Journal of Geophysical Research* **102**(D24), 28901–28909.

Bird, R. E. & Riordan, C. (1986), 'Simple solar spectral model for direct and diffuse irradiance on horizontal and tilted planes at the earth's surface for cloudless atmospheres', *Journal of Climate and Applied Meteorology* **25**(1), 87–97.

Box, J. E., Fettweis, X., Stroeve, J. C., Tedesco, M., Hall, D. K. & Steffen, K. (2012), 'Greenland ice sheet albedo feedback: thermodynamics and atmospheric drivers', *The Cryosphere* **6**(4), 821–839.

Briegleb, B., Minnis, P., Ramanathan, V. & Harrison, E. (1986), 'Comparison of regional clear-sky albedos inferred from satellite observations and model computations', *Journal of Climate and Applied Meteorology* **25**, 214–226.

Budyko, M. (1969), 'The effect of solar radiation variations on the climate of the earth', *Tellus* **5**, 611–619.

Carroll, J. J. & Fitch, B. W. (1981), 'Effects of solar elevation and cloudiness on snow albedo at the south pole', *Journal of Geophysical Research* **86**(C6), 5271–5276.

Cavalieri, D., Parkinson, C., Gloersen, P. & Zwally, H. J. (1996), *Sea Ice Concentrations from Nimbus-7 SMMR and DMSP SSM/I-SSMIS Passive Microwave Data, 1982-2009*, National Snow and Ice Data Center, Boulder, Colorado, USA. updated yearly.

Clark, R., Swayze, G., Wise, R., Livo, E., Hoefen, T., Kokaly, R. & Sutley, S. (2007), 'USGS digital spectral library splib06a', Digital Data Series 231.
URL: *http://speclab.cr.usgs.gov/spectral-lib.html*

Comiso, J. (2001), 'Satellite-observed variability and trend in sea-ice extent, surface temperature, albedo and clouds in the Arctic.', *Annals of Glaciology* **33**(1), 457–473.

Curry, J. A., Rossow, W. B., Randall, D. & Schramm, J. L. (1996), 'Overview of arctic cloud and radiation characteristics', *Journal of Climate* **9**, 1731–1764.

Curry, J., Schramm, J., Perovich, D. & Pinto, J. (2001), 'Applications of SHEBA/FIRE data to evaluation of snow/ice albedo parameterizations', *Journal of Geophysical Research* **106**(D14), 15345–15355.

DeAbreu, R., Key, J., Maslanik, J., Serreze, M. & LeDrew, E. (1994), 'Comparison of in situ and AVHRR-derived broadband albedo over arctic sea ice', *Arctic* **47**(3), 288–297.

Dobson, M., Ulaby, F., Pierce, L., Sharik, T., Bergen, K., Kellndorfer, J., Kendra, J., Li, E., Lin, Y.-C., Nashashibi, A., Sarabandi, K. & Siqueira, P. (1995), 'Estimation of forest biophysical characteristics in Northern Michigan with SIR-C/X-SAR', *IEEE Transactions on Geoscience and Remote Sensing* **33**(4), 877–895.

Doherty, S., Warren, S., Grenfell, T., Clarke, A. & Brandt, R. (2010), 'Light-absorbing impurities in arctic snow', *Atmospheric Chemistry and Physics* **10**, 11647–11680.

Domine, F., Salvatori, R., Legagneux, L., Salzano, R., Fily, M. & Casacchia, R. (2006), 'Correlation between the specific surface area and the short wave infrared (SWIR) reflectance of snow', *Cold Regions Science and Technology* **46**(1), 60 – 68.

Dozier, J. (1989), 'Spectral signature of alpine snow cover from the landsat thematic mapper', *Remote Sensing of Environment* **28**, 9–22.

Dybbroe, A., Thoss, A. & Karlsson, K.-G. (2005), 'SAFNWC AVHRR cloud detection and analysis using dynamic thresholds and radiative transfer modelling part I: Algorithm description', *Journal of Applied Meteorology* **44**, 39–54.

Farr, T. G., Rosen, P. A., Caro, E., Crippen, R., Duren, R., Hensley, S., Kobrick, M., Paller, M., Rodriguez, E., Roth, L., Seal, D., Shaffer, S., Shimada, J., Umland, J., Werner, M., Oskin, M., Burbank, D. & Alsdorf, D. (2007), 'The shuttle radar topography mission', *Reviews of Geophysics* **45**(2), n/a–n/a.

Fetterer, F. & Untersteiner, N. (1998), 'Observations of melt ponds on arctic sea ice', *Journal of Geophysical Research: Oceans* **103**(C11), 24821–24835.

Flanner, M. G. & Zender, C. S. (2006), 'Linking snowpack microphysics and albedo evolution', *Journal of Geophysical Research* **111**(D12).

Fritz, S., Krishna Rao, P. & Weinstein, M. (1962), 'Satellite measurements of reflected solar energy and the energy received at the ground', *Journal of the Atmospheric Sciences* **21**(2), 141–151.

Garcia, D. (2010), 'Robust smoothing of gridded data in one and higher dimensions with missing values', *Computational Statistics and Data Analysis* **54**(4), 1167–1178.

Gardner, A. S. & Sharp, M. J. (2010), 'A review of snow and ice albedo and the development of a new physically based broadband albedo parameterization', *Journal of Geophysical Research* **115**, F01009.

Gascard, J.-C., Bruemmer, B., Offermann, M., Doble, M., Wadhams, P., Forsberg, R., Hanson, S., Skourup, H., Gerland, S., Nicolaus, M., Metaxian, J.-P., Grangeon, J., Haapala, J., Rinne, E., Haas, C., Heygster, G., Jakobson, E., Palo, T., Wilkinson, J., Kaleschke, L., Claffey, K., Elder, B. & Bottenheim, J. (2008), 'Exploring arctic transpolar drift during dramatic sea ice retreat', *EOS* **89**(3), 21–28.

Grenfell, T. C. & Maykut, G. A. (1977), 'The optical properties of ice and snow in the arctic basin', *Journal of Climatology* **18**(80), 445–463.

Grenfell, T. & Warren, S. (1999), 'Representation of a nonspherical ice particle by a collection of independent spheres for scattering and absorption of radiation', *Journal of Geophysical Research* **104**, 31697–31709.

Hall, A. (2004), 'The role of surface albedo feedback in climate', *Journal of Climate* **17**, 1550–1568.

Heidinger, A. K., Straka, III, W. C., Molling, C. C., Sullivan, J. T. & Wu, X. (2010), 'Deriving an inter-sensor consistent calibration for the avhrr solar reflectance data record', *International Journal of Remote Sensing* **31**(24), 6493–6517.

Kalitin, N. N. (1930), 'The measurements of the albedo of a snow cover', *Monthly Weather Review* **58**(2), 59–61.

Kanamitsu, M., Ebisuzaki, W., Woollen, J., Yang, S.-K., Hnilo, J., Fiorino, M. & Potter, G. L. (2002), 'NCEP-DEO AMIP-II Reanalysis (R-2)', *Bulletin of the American Meteorological Society* **83**, 1631–1643.

Karlsson, K.-G. & Dybbroe, A. (2010), 'Evaluation of arctic cloud products from the EUMETSAT climate monitoring satellite application facility based on CALIPSO-CALIOP observations', *Atmospheric Chemistry and Physics* **10**(4), 1789–1807.

Kaufman, Y. & Gao, B.-C. (1992), 'Remote sensing of water vapor in the near IR from EOS/MODIS', *IEEE Transactions on Geoscience and Remote Sensing* **30**(5), 871–884.

Kaufman, Y. J. & Tanré, D. (1996), 'Strategy for direct and indirect methods for correcting the aerosol effect on remote sensing: From {AVHRR} to EOS-MODIS ', *Remote Sensing of Environment* **55**(1), 65 – 79.

Key, J. R., Wang, X., Stoeve, J. C. & Fowler, C. (2001), 'Estimating the cloudy-sky albedo of sea ice and snow from space', *Journal of Geophysical Research* **106**(D12), 12489–12497.

Klein, A. G. & Stroeve, J. (2002), 'Development and validation of a snow albedo algorithm for the MODIS instrument', *Annals of Glaciology* **34**(1), 45–52.

Knap, W. (2012), 'Basic measurements of radiation at station Cabauw (2012-09), knmi, de bilt, the netherlands'.

Kokhanovsky, A., Aoki, T., Hachikubo, A., Hori, M. & Zege, E. (2005), 'Reflective properties of natural snow: approximate asymptotic theory versus in situ measurements', *IEEE Transactions on Geoscience and Remote Sensing* **43**(7), 1529–1535.

Konzelmann, T. & Ohmura, A. (1995), 'Radiative fluxes and their impact on the energy balance of the Greenland Ice Sheet', *Journal of Glaciology* **41**, 490–502.

Kung, E. C., Bryson, R. A. & Lenschow, D. H. (1964), 'Study of a continental surface albedo on the basis of flight measurements and structure of the earth's surface cover over North America', *Monthly Weather Review* **92**(12), 543–564.

Kuusinen, N., Kolari, P., Levula, J., Porcar-Castell, A., Stenberg, P. & Berninger, F. (2012), 'Seasonal variation in boreal pine forest albedo and effects of canopy snow on forest reflectance', *Agricultural and Forest Meteorology* **164**(0), 53 – 60.

Kuusk, A. (2001), 'A two-layer canopy reflectance model', *Journal of Quantitative Spectroscopy and Radiative Transfer* **71**(1), 1 – 9.

Kwok, R. & Rothrock, D. A. (2009), 'Decline in arctic sea ice thickness from submarine and ICESat records: 1958-2008', *Geophysical Research Letters* **36**(15), L15501–.

Laine, V. (2004), 'Arctic sea ice regional albedo variability and trends, 1982-1998', *Journal of Geophysical Research* **109**, C06027, doi:10.1029/2003JC001818.

Legagneux, L., Cabanes, A. & Domine, F. (2002), 'Measurement of the specific surface area of 176 snow samples using methane adsorption at 77 k', *Journal of Geophysical Research: Atmospheres* **107**(D17), ACH 5–1–ACH 5–15.

Legagneux, L., Taillandier, A.-S. & Domine, F. (2004), 'Grain growth theories and the isothermal evolution of the specific surface area of snow', *Journal of Applied Physics* **95**(11), 6175–6184.

Li, W., Stamnes, K., Chen, B. & Xiong, X. (2001), 'Snow grain size retrieved from near-infrared radiances at multiple wavelengths', *Geophysical Research Letters* **28**, 1699–1702.

Li, Z. & Garand, L. (1994), 'Estimation of surface albedo from space: A parameterization for global application', *Journal of Geophysical Research: Atmospheres* **99**(D4), 8335–8350.

Liang, S. (2000), 'Narrowband to broadband conversions of land surface albedo I: Algorithms', *Remote Sensing of Environment* **76**, 213–238.

Liang, S., Fang, H., Chen, M., Shuey, C. J., Walthall, C., Daughtry, C., Morisette, J., Schaaf, C. & Strahler, A. (2002), 'Validating MODIS land surface reflectance and albedo products: methods and preliminary results', *Remote Sensing of Environment* **83**, 149–162.

Light, B., Maykut, G. A. & Grenfell, T. C. (2004), 'A temperature-dependent, structural-optical model of first-year sea ice', *Journal of Geophysical Research: Oceans* **109**(C6).

Liljequist, G. (1956), Energy exchange of an antarctic snow field: Shortwave radiation (Maudheim 71 ° 03' S, 10 ° 56' W), *in* 'Norwegian-British-Swedish Antarctic Expedition, 1949-1952', Norsk Polarinstitutt.

Lindsay, R. W. & Rothrock, D. (1994), 'Arctic sea ice albedo from AVHRR', *Journal of Climate* **7**, 1737–1749.

Loew, A. & Govaerts, Y. (2010), 'Towards multidecadal consistent Meteosat surface albedo time series', *Remote Sensing* **2**(4), 957–967.

Lucht, W., Hymana, A. H., Strahler, A. H., Barnsley, M. J., Hobson, P. & Muller, J.-P. (2000), 'A comparison of satellite-derived spectral albedos to ground-based broadband albedo measurements modeled to satellite spatial scale for a semidesert landscape', *Remote Sensing of Environment* **74**, 85–98.

Lucht, W., Schaaf, C. & Strahler, A. (2000), 'An algorithm for the retrieval of albedo from space using semiempirical BRDF models', *IEEE Transactions on Geoscience and Remote Sensing* **38**(2), 977–998.

Manninen, T., Andersson, K. & Riihelä, A. (2011), Topography correction of the CM-SAF surface albedo product SAL, *in* 'Proceedings of the 2011 EUMETSAT Meteorological Satellite Conference, Oslo, Norway'.

Manninen, T. & Stenberg, P. (2009), 'Simulation of the effect of snow covered forest floor on the total forest albedo', *Agricultural and Forest Meteorology* **149**(2), 303 – 319.

Markus, T., Stroeve, J. C. & Miller, J. (2009), 'Recent changes in arctic sea ice melt onset, freezeup, and melt season length', *Journal of Geophysical Research* **114**(C12), C12024–.

Maslanik, J. A., Fowler, C., Stroeve, J., Drobot, S., Zwally, J., Yi, D. & Emery, W. (2007), 'A younger, thinner arctic ice cover: Increased potential for rapid, extensive sea-ice loss', *Geophysical Research Letters.* **34**(24), L24501–.

Maslanik, J., Fowler, C., Key, J., Scambos, T., Hutchinson, T. & Emery, W. (1997), 'AVHRR-based Polar Pathfinder products for modeling applications', *Annals of Glaciology* **25**, 388–392.

Matheron, G. (1963), 'Principles of geostatistics', *Economic Geology* **58**(8), 1246–1266.

Maykut, G. A. (1982), 'Large-scale heat exchange and ice production in the central Arctic', *Journal of Geophysical Research: Oceans* **87**(C10), 7971–7984.

Nicodemus, F. E. (1970), 'Reflectance nomenclature and directional reflectance and emissivity.', *Applied Optics* **9**(6), 1474–1475.

Niu, X. & Pinker, R. T. (2011), 'Radiative fluxes at Barrow, Alaska: A satellite view', *Journal of Climate* **24**(21), 5494–5505.

Nolin, A. & Dozier, J. (2000), 'A hyperspectral method for remotely sensing the grain size of snow', *Remote Sensing of Environment* **74**(2), 207–216.

Nordberg, W., Bandeen, W. R., Conrath, B. J., Kunde, V. & Persano, I. (1962), 'Preliminary results of radiation measurements from the

TIROS III meteorological satellite', *Journal of the Atmospheric Sciences* **19**(1), 20–30.

Parkinson, C. L. & Cavalieri, D. (2008), 'Arctic sea ice variability and trends, 1979–2006', *Journal of Geophysical Research* **113**, C07003.

Peltoniemi, J. I., Kaasalainen, S., Näränen, J., Rautiainen, M., Stenberg, P., Smolander, H., Smolander, S. & Voipio, P. (2005), 'BRDF measurement of understory vegetation in pine forests: dwarf shrubs, lichen, and moss', *Remote Sensing of Environment* pp. 343–354.

Perovich, D., Grenfell, T., Light, B. & Hobbs, P. (2002), 'Seasonal evolution of the albedo of multiyear arctic sea ice', *Journal of Geophysical Research* **107**(C10), 1–13.

Perovich, D. K. (1996), The optical properties of sea ice, Technical report, Cold Regions Research and Engineering Lab, Hanover, New Hampshire, United States. 31 pages.

Perovich, D. K. & Polashenski, C. (2012), 'Albedo evolution of seasonal arctic sea ice', *Geophysical Research Letters* **39**(8), L08501–.

Perovich, D., Nghiem, S., Markus, T. & Schweiger, A. (2007), 'Seasonal evolution and interannual variability of the local solar energy absorbed by the arctic sea ice-ocean system', *Journal of Geophysical Research* **112**, doi:10.1029/2006JC003558.

Pielke, R. A. & Vidale, P. L. (1995), 'The boreal forest and the polar front', *Journal of Geophysical Research: Atmospheres* **100**(D12), 25755–25758.

Rahman, H. & Dedieu, G. (1994), 'Smac: a simplified method for the atmospheric correction of satellite measurements in the solar spectrum', *International Journal of Remote Sensing* **15**(1), 123–143.

Rampal, P., Weiss, J. & Marsan, D. (2009), 'Positive trend in the mean speed and deformation rate of Arctic sea ice, 1979–2007', *Journal of Geophysical Research: Oceans* **114**(C5).

Raschke, E., Vonder Haar, T. H., Bandeen, W. R. & Pasternak, M. (1973), 'The annual radiation balance of the earth-atmosphere system during 1969-70 from Nimbus 3 measurements', *Journal of the Atmospheric Sciences* **30**(3), 341–364.

Riihelä, A., Lahtinen, P. & Hakala, T. (2011), 'The radiation, snow characteristics and albedo at summit (RASCALS) expedition report', FMI Reports 2011:8. 41 pages.
URL: *https://helda.helsinki.fi/handle/10138/28678*

Robock, A. & Kaiser, D. (1985), 'Satellite-observed reflectance of snow and clouds', *Monthly Weather Review* **113**(11), 2023–2029.

Román, M. O., Schaaf, C. B., Woodcock, C. E., Strahler, A. H., Yang, X., Braswell, R. H., Curtis, P. S., Davis, K. J., Dragoni, D., Goulden, M. L., Gu, L., Hollinger, D. Y., Kolb, T. E., Meyers, T. P., Munger, J. W., Privette, J. L., Richardson, A. D., Wilson, T. B. & Wofsy, S. C. (2009), 'The MODIS (collection v005) BRDF/albedo product: Assessment of spatial representativeness over forested landscapes', *Remote Sensing of Environment* **113**(11), 2476–2498.

Roujean, J.-L., Leroy, M. & Deschamps, P.-Y. (1992), 'A bidirectional reflectance model of the earth's surface for the correction of remote sensing data', *Journal of Geophysical Research* **97**(18), 20455–20468.

Roujean, J.-L., Manninen, T., Sukuvaara, T., Peltoniemi, J. I., Kaasalainen, S., Hautecoeur, O., Lahtinen, P., Riihelä, A., Siljamo, N., Lötjönen, M., Karjalainen, T., Kontu, A., Suokanerva, H., Aulamo, O., Lemmetyinen, J., Suomalainen, J., Hakala, T., Kaartinen, H., Thölix, L., Meinander, O. & Karhu, J. (2010), 'SNORTEX: remote sensing measurement of snowmelt in european boreal forest', *iLEAPS Newsletter* **9**, 56–58.

Salomonson, V., Barnes, W., Maymon, P., Montgomery, H. & Ostrow, H. (1989), 'MODIS: advanced facility instrument for studies of the earth as a system', *IEEE Transactions on Geoscience and Remote Sensing* **27**(2), 145–153.

Schaepman-Strub, G., Schaepman, M. E., Painter, T. H., Dangel, S. & Martonchik, J. V. (2006), 'Reflectance quantities in optical remote sensing – definitions and case studies', *Remote Sensing of Environment* **103**, 27–42.

Serreze, M., Barrett, A., Stroeve, J., Kindig, D. & Holland, M. (2009), 'The emergence of surface-based arctic amplification', *The Cryosphere* **3**, 11–19.

Stowe, L. L., Jacobowitz, H., Ohring, G., Knapp, K. R. & Nalli, N. R. (2002), 'The advanced very high resolution radiometer (AVHRR) pathfinder atmosphere (PATMOS) climate dataset: Initial analyses and evaluations', *Journal of Climate* **15**(11), 1243–1260.

Stroeve, J. (2001), 'Assessment of Greenland albedo variability from the Advanced Very High Resolution Radiometer Polar Pathfinder data set', *Journal of Geophysical Research* **106**(D24), 33989–34006.

Stroeve, J., Holland, M. M., Meier, W., Scambos, T. & Serreze, M. (2007), 'Arctic sea ice decline: Faster than forecast', *Geophysical Research Letters* **34**(9), L09501–.

Stroeve, J., Nolin, A. & Steffen, K. (1997), 'Comparison of AVHRR-derived and in situ surface albedo over the greenland ice sheet', *Remote Sensing of Environment* **62**, 262–276.

Susaki, J., Yasuoka, Y., Kajiwara, K., Honda, Y. & Hara, K. (2007), 'Validation of MODIS albedo products of paddy fields in japan', *IEEE Transactions on Geoscience and Remote Sensing* **45**(1), 206 –217.

Toledano, C., Cachorro, V., Gausa, M., Stebel, K., Aaltonen, V., Berjón, A., de Galisteo, J. O., de Frutos, A., Bennouna, Y., Blindheim, S., Myhre, C., Zibordi, G., Wehrli, C., Kratzer, S., Hakansson, B., Carlund, T., de Leeuw, G., Herber, A. & Torres, B. (2012), 'Overview of sun photometer measurements of aerosol properties in Scandinavia and Svalbard', *Atmospheric Environment* **52**(0), 18 – 28.

Tomasi, C., Lupi, A., Mazzola, M., Stone, R. S., Dutton, E. G., Herber, A., Radionov, V. F., Holben, B. N., Sorokin, M. G., Sakerin, S. M., Terpugova, S. A., Sobolewski, P. S., Lanconelli, C., Petkov,

B. H., Busetto, M. & Vitale, V. (2012), 'An update on polar aerosol optical properties using POLAR-AOD and other measurements performed during the international polar year', *Atmospheric Environment* **52**(0), 29 – 47.

Vonder Haar, T. H. & Suomi, V. E. (1969), 'Satellite observations of the earth's radiation budget', *Science* **163**(3868), 667–668.

Wang, M. & Overland, J. E. (2012), 'A sea ice free summer arctic within 30 years: An update from cmip5 models', *Geophysical Research Letters* **39**(18), L18501–.

Wang, X. & Key, J. R. (2005), 'Arctic surface, cloud, and radiation properties based on the avhrr polar pathfinder dataset. part ii: Recent trends', *J. Climate* **18**(14), 2575–2593.

Warren, S., Brandt, R. & Hinton, P. (1998), 'Effect of surface roughness on bidirectional reflectance of antarctic snow', *Journal of Geophysical Research* **103**(E11), 25789–25807.

Warren, S. G. (1982), 'Optical properties of snow', *Reviews of Geophysics and Space Physics* **20**(1), 67–89.

Warren, S. G. & Wiscombe, W. J. (1980), 'A model for the spectral albedo of snow. II: Snow containing atmospheric aerosols', *Journal of the Atmospheric Sciences* **37**, 2734–2744.

Wessel, P. & Smith, W. H. F. (1996), 'A global, self-consistent, hierarchical, high-resolution shoreline database', *Journal of Geophysical Research* **101**(B4), 8741–8743.

West, A. E., Keen, A. B. & Hewitt, H. T. (2013), 'Mechanisms causing reduced arctic sea ice loss in a coupled climate model', *The Cryosphere* **7**(2), 555–567.

West, G. B., Brown, J. H. & Enquist, B. J. (1999), 'The fourth dimension of life: Fractal geometry and allometric scaling of organisms', *Science* **284**(5420), 1677–1679.

Wiscombe, W. J. & Warren, S. G. (1980), 'A model for the spectral albedo of snow, I: Pure snow', *Journal of the Atmospheric Sciences* **37**, 2712–2733.

Wu, A., Li, Z. & Cihlar, J. (1995), 'Effects of land cover type and greenness on Advanced Very High Resolution Radiometer bidirectional reflectances: Analysis and removal', *Journal of Geophysical Research* **100**(D5), 9179–9192.

Xiong, X., Stamnes, K. & Lubin, D. (2002), 'Surface albedo over the arctic ocean derived from AVHRR and its validation with SHEBA data', *Journal of Applied Meteorology* **41**, 413–425.

Ångström, A. (1919), 'A new instrument for measuring sky radiation', *Monthly Weather Review* **11**, 795–797.

Ångström, A. (1925), 'The albedo of various surfaces of ground', *Geografiska Annaler* **7**, 323–342.